Stem Cell Reports
Article

ISSCR

OPEN ACCESS

Signaling-Dependent Control of Apical Membrane Size and Self-Renewal in Rosette-Stage Human Neuroepithelial Stem Cells

Jan-Philip Medelnik,[1,2,3,*] Kathleen Roensch,[2,3] Satoshi Okawa,[4] Antonio del Sol,[4] Osvaldo Chara,[5,6] Levan Mchedlishvili,[2,3,7] and Elly M. Tanaka[1,2,3]

[1]Research Institute for Molecular Pathology (IMP), Vienna Biocenter (VBC), Campus-Vienna-Biocenter 1, 1030 Vienna, Austria
[2]DFG Research Center for Regenerative Therapies, Technische Universität Dresden, Fetscherstraße 105, 01307 Dresden, Germany
[3]Max Planck Institute of Molecular Cell Biology and Genetics, Pfotenhauerstraße 108, 01307 Dresden, Germany
[4]Computational Biology Group, Luxembourg Centre for Systems Biomedicine, University of Luxembourg, 6, Avenue du Swing, Belvaux 4367, Luxembourg
[5]Center for Information Services and High Performance Computing (ZIH), Technische Universität Dresden, 01062 Dresden, Germany
[6]Systems Biology Group (SysBio), Instituto de Física de Líquidos y Sistemas Biológicos (IFLySIB), CONICET, Universidad Nacional de La Plata (UNLP), B1900BTE, La Plata, Argentina
[7]Present address: University Hospital Greifswald Department of Neurosurgery, Sauerbruchstraße, 17475 Greifswald, Germany
*Correspondence: jan.medelnik@imp.ac.at
https://doi.org/10.1016/j.stemcr.2018.04.018

SUMMARY

In the developing nervous system, neural stem cells are polarized and maintain an apical domain facing a central lumen. The presence of apical membrane is thought to have a profound influence on maintaining the stem cell state. With the onset of neurogenesis, cells lose their polarization, and the concomitant loss of the apical domain coincides with a loss of the stem cell identity. Little is known about the molecular signals controlling apical membrane size. Here, we use two neuroepithelial cell systems, one derived from regenerating axolotl spinal cord and the other from human embryonic stem cells, to identify a molecular signaling pathway initiated by lysophosphatidic acid that controls apical membrane size and consequently controls and maintains epithelial organization and lumen size in neuroepithelial rosettes. This apical domain size increase occurs independently of effects on proliferation and involves a serum response factor-dependent transcriptional induction of junctional and apical membrane components.

INTRODUCTION

Epithelial polarization and organization of a central lumen is a defining aspect of nervous system formation. During early vertebrate neurulation the neural plate is formed, which subsequently undergoes folding to form the neural tube. At early stages, before and shortly after closure of the neural tube, the neuroepithelium consists of self-renewing, tight-junction-forming neural progenitor cells (NPCs) whose apical domains all face toward a central lumen that contains the cerebrospinal fluid. At later stages, junctional complexes are remodeled; cells lose tight junctions and their polarized morphology, and at the same time the onset of neuronal differentiation begins (Aaku-Saraste et al., 1996).

The capability of tight-junction-containing NPCs to organize into polarized, lumen-containing structures is also evident during neural organoid formation (Eiraku et al., 2011; Meinhardt et al., 2014) and in two-dimensional cultures of mouse embryonic day 8 (E8) primary neural plate cell explants that spontaneously self-cluster to form two-dimensional mini-lumina termed "neural rosettes" (Elkabetz et al., 2008). Neural rosettes consist of small cellular units in which the NPCs all orient their apical domain to a common lumen-like center. Due to their self-organizing capacity, neural rosettes can be regarded as *in vitro*, two-dimensional versions of the neural tube. Similar to the gradual loss of neural stem cell identity in the developing neural tube, the ability of neuroepithelial cell explants derived from E8 mouse embryos to organize in rosettes is also restricted to a short window of early neural development prior to a loss of polarization. It has been difficult to maintain rosettes in culture as they tend to spontaneously progress toward more differentiated, less polarized phenotypes (Elkabetz et al., 2008).

An alternative source of rosette-forming, tight-junction-containing neuroepithelium has been mouse and human embryonic stem cells (hESCs) early after neural lineage induction. The early rosette-forming neuroepithelial state is considered an important state for stem cell differentiation, as it represents the early neural plate or neural tube stage at which cells have committed to the neural lineage but are still susceptible to instructive cues that pattern the CNS along the anterior/posterior and dorsal/ventral axes (Broccoli et al., 2014; Elkabetz et al., 2008; Li et al., 2005). In hESCs, dual inhibition of SMAD signaling by noggin/dorsomorphin and SB431542 efficiently directs cells along the neural lineage and results in rosette formation (Chambers et al., 2009; Zhou et al., 2010). However, upon passaging, cells successively form smaller rosettes in which cell polarization and tight junctions become reduced over time until the neuroepithelial cell state is lost. Elkabetz et al. (2008) reported that addition of SHH and the Notch signaling agonists Delta and Jagged1 during

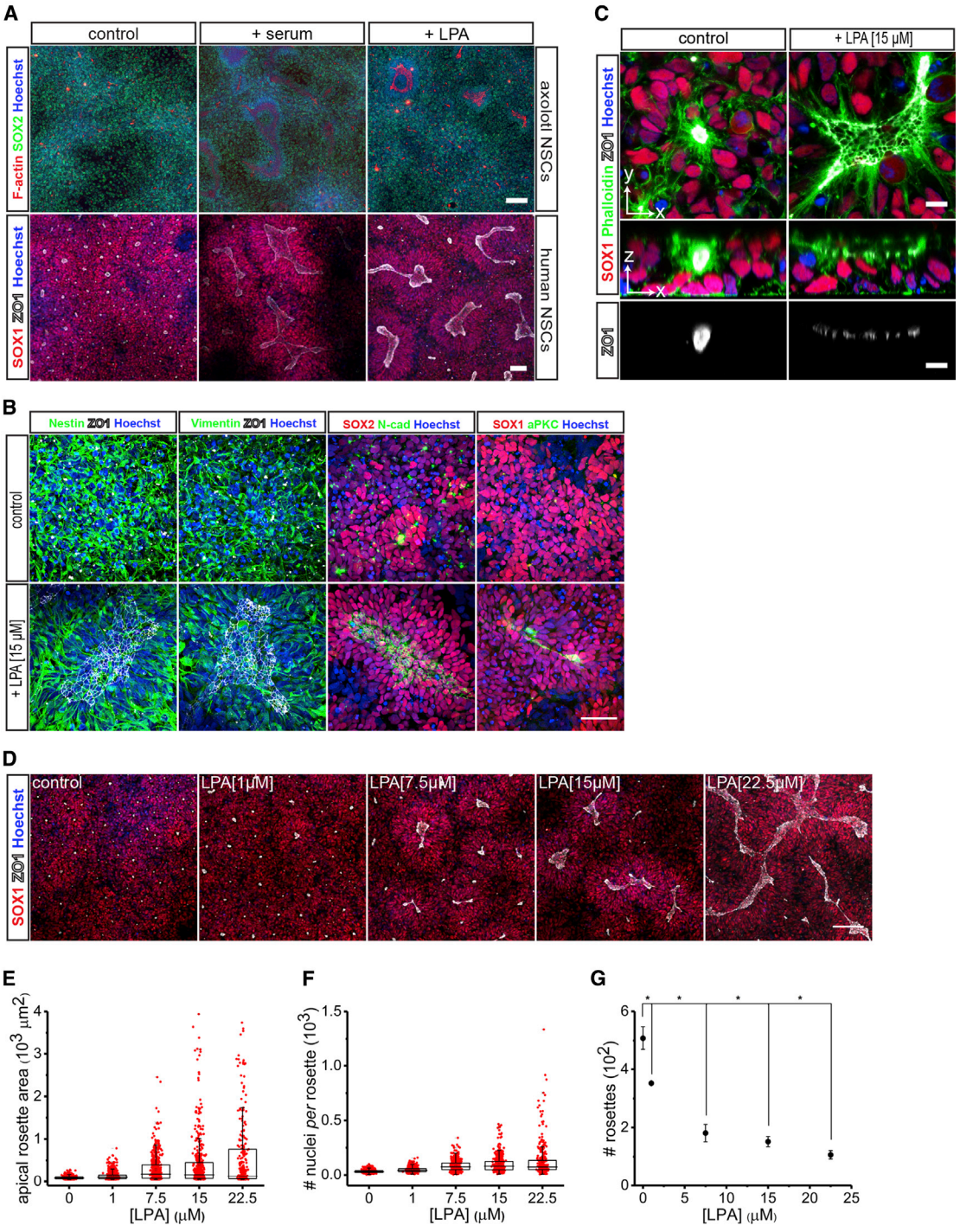

Figure 1. Serum and LPA Induce Large Rosette Formation in Cultured Axolotl and Human NPCs

(A) Immunostaining of axolotl- and hESC-derived NPCs for SOX2 (upper panels), and SOX1 and ZO-1 (lower panels) shows induction of large rosette formation in the presence of serum or LPA. F-actin in axolotl NPCs was stained with Alexa Fluor 647 phalloidin. Scale bars, 200 μm (upper panels) and 100 μm (lower panels).

(B and C) Immunostaining of hESC-derived NPCs for Nestin, Vimentin, SOX1, SOX2, N-cadherin, aPKC and ZO-1. F-actin was labeled with Alexa Fluor 488 phalloidin. y-x images represent top view and z-x images side view. Scale bars, 50 μm (B) and 10 μm (C).

(D) Immunostaining of NPCs that have formed enlarged rosettes after 18 hr of exposure to different LPA concentrations (0–22.5 μM) for SOX1 and ZO-1. Scale bar, 100 μm.

(legend continued on next page)

plating of rosette-forming NPCs could prolong the rosette-forming state for approximately four passages by presumably promoting self-renewing cell divisions.

Few studies have identified signaling factors that control growth and expansion of the luminal neural tube-like area independent of cell proliferation, and beyond the factors mentioned above there are no known factors that specifically sustain a large rosette-forming neuroepithelial state. Identification of factors that can sustain/promote neuroepithelial lumen formation independently of or parallel to self-renewing divisions should have a profound effect on propagating the neural rosette-forming state and might forestall the timely differentiation to later-stage neural progenitors/committed cells. Interestingly, the sustained self-renewal of early neuroepithelial cells is a characteristic feature of spinal cord regeneration in the axolotl, where spinal cord lesions induce cells to enter the neuroepithelial state. This state is sustained and self-renews for at least 2 weeks to yield an outgrowth of the severed spinal cord tube (Rodrigo Albors et al., 2015; Rost et al., 2016).

Given the importance of the tight-junction-containing early neuroepithelial state during neural tube formation/regeneration in the axolotl, we sought to identify a molecular factor that promotes expansion of the apical lumen in neuroepithelial rosette cells. Here we have identified lysophosphatidic acid (LPA) as a molecule that can cause an expansion of the apical domain of axolotl and human NPCs and a growth of the rosette luminal area independent of cell proliferation. Continuous treatment of hESC-derived NPCs with LPA yields the propagation of the rosette-forming state for at least 52 passages. Correspondingly, we see a suppression of neuronal differentiation and sustenance of the SOX2$^+$, proliferative state. LPA acts through Rho and serum response factor (SRF) to promote upregulation of tight-junction actin-related- and apically associated proteins.

RESULTS

Addition of Serum or LPA to Axolotl and Human NPCs Induces Rosette Enlargement

Axolotl spinal cord regeneration is a unique system in which an injury-initiated wound response induces the self-renewal and expansion of NPCs that grow a lumen-containing neural tube, which can recapitulate neural patterning (Rodrigo Albors et al., 2015; Walder et al., 2003). A key extracellular mediator of the injury response is serum. In studies of limb regeneration two serum components, BMP4/7 and PDGF, were shown to induce proliferation (Wagner et al., 2017) and cell migration (Currie et al., 2016). We therefore asked whether serum and any of its major components could induce an expansion of neuroepithelial rosette formation in cultured axolotl spinal cord cells. While the two-dimensional neural rosettes do not represent closed lumina, they still represent neural tube-like structures that recapitulate many features of a true lumen and thus can be used to identify factors affecting lumen organization. We exposed axolotl spinal cord-derived SOX2$^+$ NPCs to a 3-day pulse of serum. Strikingly we observed the organization of the cells into larger rosette structures over time (Figure 1A, upper left and middle panels). To identify the serum component responsible for this effect, we assayed LPA, which is a major signaling phospholipid in serum. When we exposed cells to concentrations of LPA in a similar range compared with those measured in serum (Yung et al., 2014), we recapitulated the larger rosette phenotype similar to the phenotype observed with serum treatment (Figure 1A, upper right panel). We concluded that LPA is a serum-borne signaling molecule that can induce rosette enlargement in axolotl spinal cord NPCs. We next asked whether the action of LPA represents a conserved signaling pathway that can regulate rosette lumen size in other vertebrate neuroepithelia. We therefore tested whether serum and LPA induced an increase in rosette size in hESC-derived NPCs. We implemented a modified version of a three-dimensional dual SMAD signaling inhibition neural differentiation protocol, which efficiently converted hESCs into small rosette-forming SOX1$^+$ NPCs (Khattak et al., 2015) (Figures 1A [lower left panel] and S1). Upon incubation with serum or LPA, the human NPCs reorganized to form larger rosettes within 18–24 hr, indicating that the signaling pathway leading to larger rosette structures is conserved between axolotl and human NPCs (Figure 1A, lower middle and right panels).

Human NPCs Express Early NSC Markers and Exhibit Apical to Basal Polarity

Rosette NPCs are considered to represent a neural stem cell (NSC) type whose lumen-organizing capacity and neuroepithelial marker expression strongly resembles early neuroepithelium at the neural plate stage (Elkabetz et al., 2008; Li

(E and F) Quantification of the frequencies of the apical rosette lumen size areas in μm^2 and the number of SOX1$^+$ cells per rosette at different LPA levels. Red dots indicate individual apical rosette lumen sizes (E) and number of SOX1$^+$ cells participating in rosette formation (F).

(G) Mean number of rosettes ± SEM per analyzed image. Statistical analysis was performed using an ANOVA test followed by Tukey's a posteriori test. *$p < 0.05$, n = 3 independent experiments.

All nuclei were labeled with Hoechst 33342. See also Figures S1 and S2.

et al., 2005). We characterized the human neural rosettes with respect to their neuroepithelial marker expression. Both control small rosette and LPA-induced large rosette NPCs expressed the intermediate filament proteins Nestin and Vimentin and the neuroectodermal transcription factors SOX1 and SOX2. Consistent with their ability to organize a lumen-like structure, the NPCs in both conditions expressed the apically localized proteins ZO-1, N-cadherin, atypical protein kinase C (aPKC), CD133 and showed enriched localization of F-actin at their apical side (Figures 1B, 1C, and S2). While control and LPA-treated NPCs expressed similar neuroepithelial and polarity markers, we observed striking differences in the spatial organization of the cells. In control rosettes the lumen exhibited a strongly constricted morphology with clustering of the ZO-1 signal into a defined point (Figure 1C, lower and middle left panels). In contrast, in the presence of LPA the luminal surface became much larger and cells adopted an unconstricted morphology in which the individual cell-cell junctions were easily recognizable by staining for ZO-1 (Figure 1C, lower and middle right panels).

LPA Increases Lumen Size in a Concentration-Dependent Manner in Human Neural Rosettes

We further assessed whether the LPA-induced rosette size increase could be regulated by incubating the cells with different LPA concentrations. Exposure of NPCs to different LPA doses over a period of 18 hr resulted in the formation of larger rosettes with larger luminal surfaces in a concentration-dependent manner (Figure 1D). We defined the lumen surface area as the entire ZO-1-positive area completely enclosed by $SOX1^+$ nuclei. Quantification revealed that distributions of apical rosette lumen area are shifted toward larger values. In particular, lower quartiles, upper quartiles, and interquartile ranges monotonically increase from 59.4, 101.6, and 42.2 μm^2 to 64.1, 760.9, and 696.9 μm^2, respectively, in response to 22.5 μM LPA (Figure 1E). We next quantified the number of $SOX1^+$ cells per rosette. Analogously with rosette lumen area, lower quartiles, upper quartiles, and interquartile ranges monotonically increase from 24, 40, and 16 to 50, 134, and 84 cells, respectively (Figure 1F). Concomitant with the increase in rosette size, the total number of rosettes per image decreased from a mean of 508 ± 39 to 106 ± 15 rosettes (Figure 1G).

Human NPCs Can Form Large Rosettes in the Absence of Cell Proliferation

We next investigated whether the LPA-mediated increase in lumen size was a consequence of increased proliferation. Depending on the cell origin and the culturing conditions, hESC-derived and induced pluripotent stem cell (iPSC)-derived NPCs have been reported to either increase or decrease their proliferation in response to LPA (Frisca et al., 2013; Hurst et al., 2008; Pebay et al., 2007). We measured proliferation in response to LPA concentrations ranging from 0.5 μM to 2.5 μM by quantifying the percentage of 5-ethynyl-2′-deoxyuridine $(EdU)^+/SOX1^+$ cells, which revealed a 66% increase in the proliferative activity of NPCs that were exposed to 0.5 μM LPA compared with the control. Concentrations higher than 0.5 μM did not further significantly increase proliferation (Figures 2A and 2B).

To test whether cells could form larger rosettes in the absence of proliferation, we blocked proliferation with the S-phase inhibitor hydroxyurea (HU). NPCs were pretreated for 12 hr with HU prior to LPA exposure (Figures 2C and 2D). After HU pretreatment, none of the cells showed EdU incorporation and LPA was added to the NPCs. Non-proliferative NPCs exposed to LPA still significantly increased their apical rosette lumen area from a mean size of 57 ± 1 μm^2 to 131 ± 7 μm^2. Control cells that were still proliferative responded to LPA with even larger rosette formation (206 ± 20 μm^2) (Figures 2E and 2F). NPCs undergo interkinetic nuclear migration. During M phase the nuclei localize toward the apical site whereas during S phase they are located more basally. Kingsbury et al. (2003) reported that nuclei of LPA-exposed ventricular zone (VZ) NPCs that were cultured in mouse E14 cerebral cortices showed displacement toward more basal regions during M phase. However, in our case immunostaining of NPCs for the mitotic marker pH3 and quantification of the distance from the apical lumen site toward the center of the surrounding pH^+ nuclei did not significantly change the position of M-phase nuclei between both conditions (Figure S3).

LPA Induces Apical Domain Enlargement of Human NPCs

To understand the changes in epithelial organization that lead to large rosette formation of NPCs, we examined rosette organization at different times after exposure of cells to 15 μM LPA. Prior to LPA exposure the NPCs were organized in small rosettes. ZO-1 could be detected at the constricted apical cell sides, which enclosed a small lumen (Figures 3A and 3B, 0 hr). Two hours after LPA administration the apical domains had slightly expanded in width (Figures 3A, 3B, and 2H). After 10 hr, the NPCs had organized in a large and connected neuroepithelial-like cell layer in which the apical domains had adopted a much broader and unconstricted morphology (Figures 3A and 3B, 10 hr). After 18 hr of exposure to LPA, the apical domain areas started to shrink and appeared more constricted. At this point, the entire morphology rather resembled a cone-shaped large rosette structure than a large, connected, and flat neuroepithelium (Figures 3A

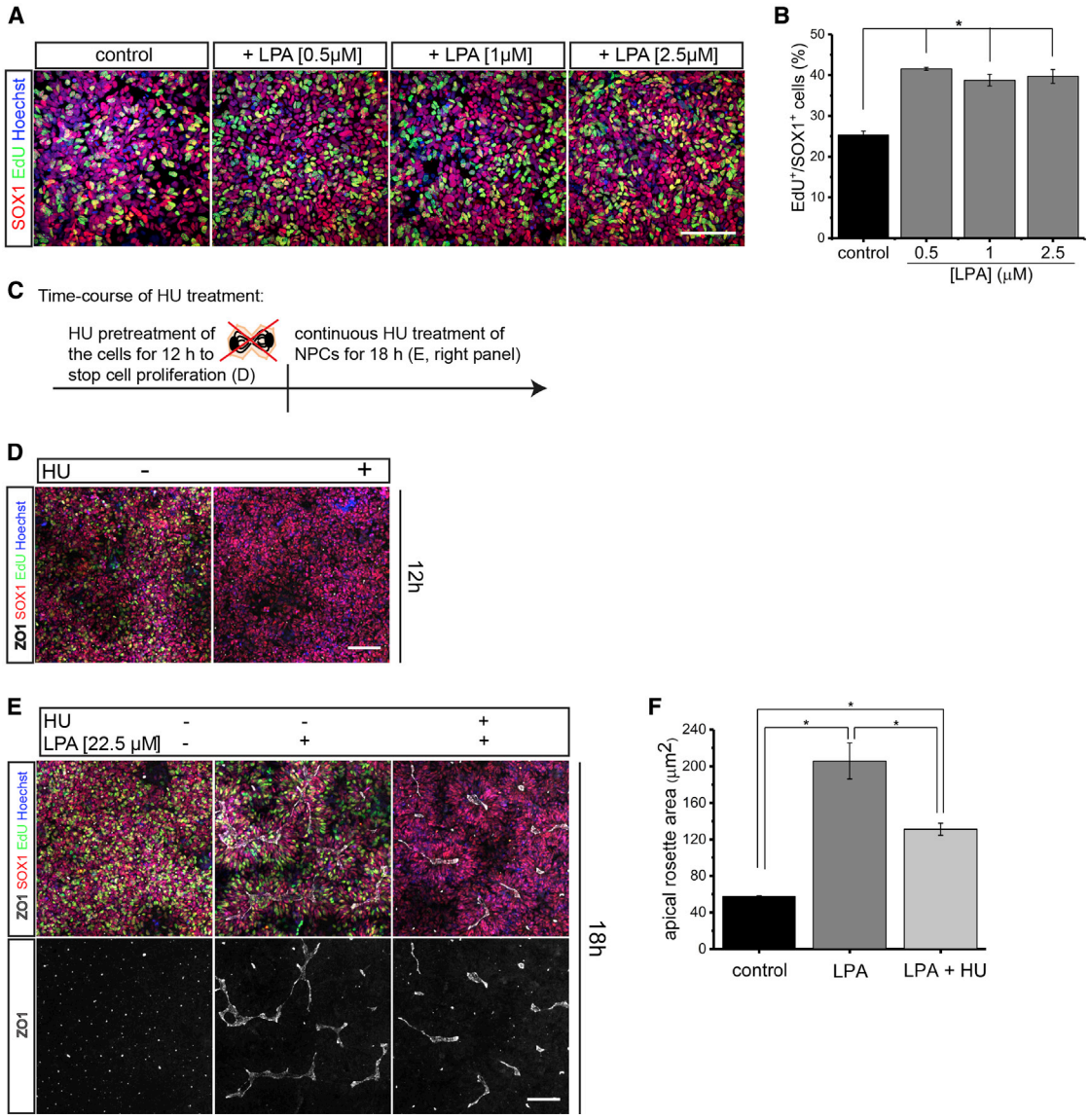

Figure 2. Cell Proliferation Is Not Required for Large Rosette Formation in Human NPCs

(A) EdU incorporation in NPCs in response to LPA. EdU signal (green) and immunofluorescence for SOX1 (red) show robust incorporation of EdU. Scale bar, 100 μm.

(B) Quantification of $EdU^+/SOX1^+$ cells. Data represent mean ± SEM, ANOVA test followed by Tukey's a posteriori test. *$p < 0.05$, $n = 3$ independent experiments.

(C) Scheme depicting the experimental setup of the cell proliferation block experiment shown in (D) and (E).

(D) NPCs were cultured for 12 hr in normal culturing medium (−) or in medium supplemented with 0.5 μM hydroxyurea (HU) (+). EdU signal (green) and immunofluorescence for SOX1 (red) and ZO-1 (white) show reduced EdU incorporation after HU treatment. Scale bar, 100 μm.

(E) Rosette formation in the absence of proliferation. NPCs were cultured in normal culturing medium (left panels), medium supplemented with 22.5 μM LPA (middle panels), or medium supplemented with 22.5 μM LPA and 0.5 μM HU (right panels). EdU signal (green) and immunofluorescence for SOX1 (red) and ZO-1 (white). Scale bar, 100 μm.

(F) Quantification of mean apical rosette lumen surface area. ANOVA test followed by Tukey's a posteriori test. Data represent mean of medians ± SEM. *$p < 0.05$, $n = 3$ independent experiments.

Prior to fixation, NPCs were incubated for 45 min with EdU (30 μM). Nuclei were labeled with Hoechst 33342 (blue). See also Figure S3.

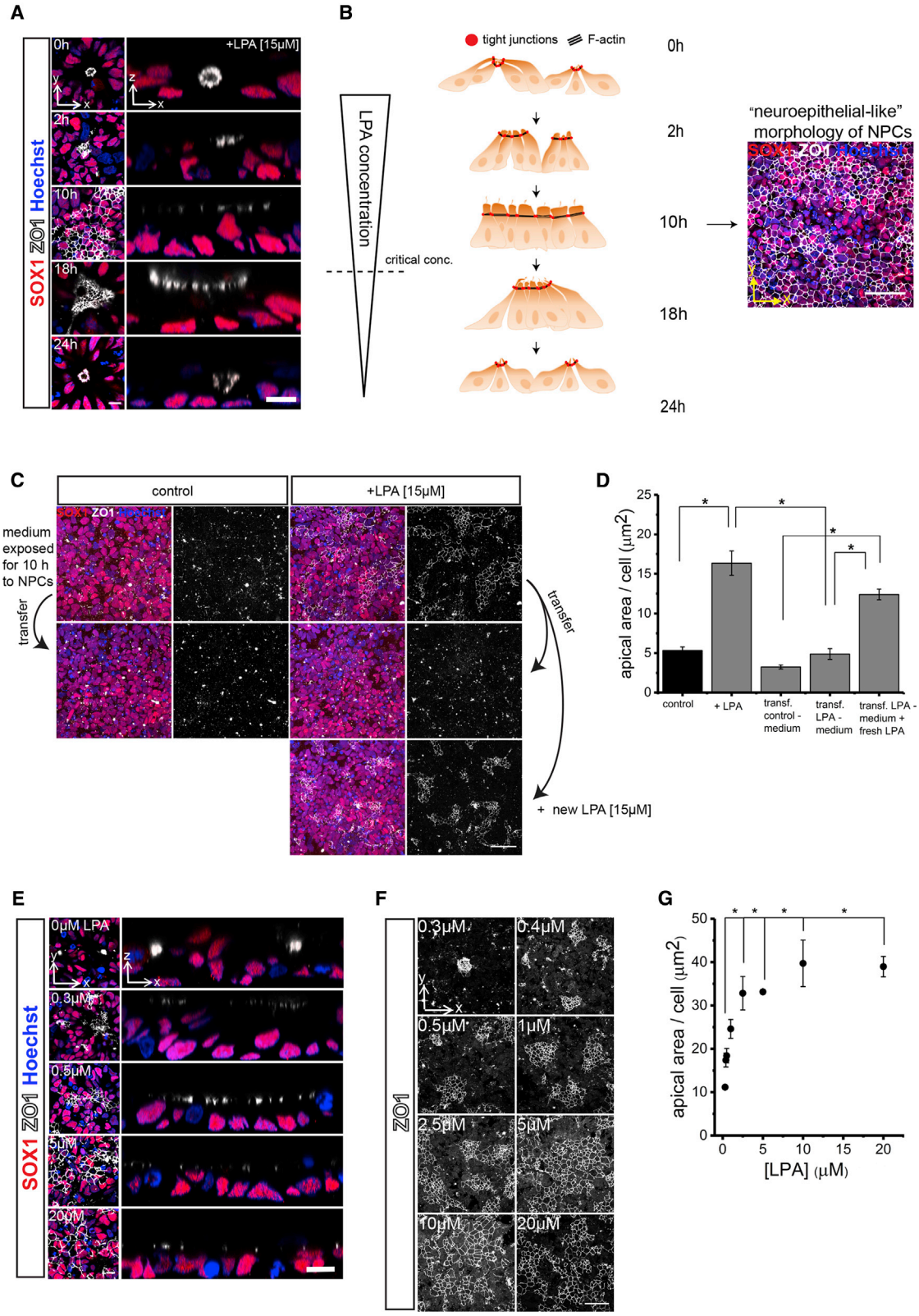

(legend on next page)

and 3B, 18 hr). At 24 hr after LPA addition, the cells had completely reverted to the constricted small rosette state (Figures 3A and 3B, 24 hr). The observations indicate that LPA dynamically regulates the epithelial organization of NPCs within 24 hr. The fact that the neuroepithelial-like morphology of the NPCs, which was observed 10 hr after LPA administration, reverted over time to smaller rosettes, suggested that LPA may not be stably maintained in the culture media over time. To investigate whether the LPA activity (15 μM) is reduced within 10 hr to a level insufficient to induce a neuroepithelial-like phenotype in NPCs *de novo*, we exposed NPCs for 10 hr to 15 μM LPA and then transferred this medium to a new culture of NPCs that had not been previously exposed to LPA. The first NPC culture revealed a strong increase in the neuroepithelial-like morphology, with a mean apical area of 16 ± 2 μm^2 per cell in LPA-treated NPCs compared with a mean apical area of 5.3 ± 0.4 μm^2 in control NPCs (Figures 3C [upper panels] and 3D). In contrast, the secondary NPCs that had been treated with medium from the first NPCs did not form larger rosettes in response to the media and only exhibited a mean apical area of 4.9 ± 0.7 μm^2 (Figures 3C [middle panels] and 3D). LPA-containing medium that had been exposed for 10 hr to NPCs and that had been supplemented with new LPA significantly induced a larger neuroepithelial-like phenotype with a mean apical area of 12.4 ± 0.7 μm^2 per cell (Figures 3C [lower panels] and 3D). The data show that LPA promotes the organization of NPCs into a large neuroepithelial-like cell layer as long as its activity within the medium is high and does not fall below a certain threshold (Figure 3B, dashed line). These data also show that LPA activity (15 μM) in the culture medium is reduced over a period of 10 hr to a level insufficient to induce rosette enlargement.

LPA Increases Apical Domain Size of Human NPCs in a Concentration-Dependent Fashion

The previous findings prompted us to investigate whether NPC apical domain size has a dose-dependent relation to the LPA concentration to which the cells are exposed. We employed a protocol whereby we exposed NPCs to stable LPA concentrations ranging from 0.3 to 20 μM for 36 hr to allow enough time for the cells to respond to LPA (see Supplemental Experimental Procedures). Immunofluorescence of the cells showed that the size of the apical domains, quantified as the areas of low ZO-1 signal intensity in between the cell-cell borders, concomitantly increased with increasing LPA concentrations. As a consequence of the apical expansion, small rosettes opened up their constricted morphology, and NPCs of adjacent rosettes started to connect their apical domains and fused into a larger connected epithelial cell layer (Figure 3E). Quantification revealed a significant increase in the average apical domain size per cell with increasing LPA concentrations (Figures 3F and 3G). Analysis of the dependency of apical domain size on the LPA concentrations was performed by a two-state model (see Supplemental Experimental Procedures). From the results we concluded that a primary effect of LPA on the NPCs is the increase in apical domain area, where 50% of the maximal area can be achieved at 0.76 μM LPA, a concentration in the range of physiological LPA concentrations present in serum. Taken together, our results indicate that the single application of LPA leads to an early expansion of apical domains and the fusion of small rosettes into a connected cell layer. As LPA is depleted from the media and apical domains start to shrink, cells segregate into rosettes that shrink in lumen area over time. The duration of the flat neuroepithelial state and the onset of the reversion back to the large and then small rosette

Figure 3. LPA Dynamically Regulates the Epithelial Organization and Increases Apical Domain Size of Human NPCs

(A) Immunostaining of NPCs that were fixed at different time points after LPA administration for SOX1 and ZO-1. y-x images represent top view and z-x images side view. Scale bars, 10 μm.

(B) Scheme depicting the changes in the epithelial organization of the NPCs over a period of 24 hr. Triangle (left side) indicates decreasing LPA activity. Dashed line indicates the critical LPA activity inside the medium required to maintain the NPCs in a large apical domain-neuroepithelial-like state. Immunostaining shows NPCs that have adopted a large neuroepithelial-like morphology after LPA treatment. Scale bar, 50 μm.

(C) Upper panels: NPCs incubated with 0.5 mL of medium (left) or medium supplemented with 15 μM LPA (right). Middle panels: NPCs exposed for 10 hr to medium in which NPCs had already been cultivated for 10 hr and that was either without LPA (left) or supplemented with LPA (right). Lower panels: NPCs exposed to culture medium for 10 hr in which NPCs had already been cultivated for 10 hr and that was supplemented with new LPA. Immunostaining of NPCs for SOX1 (red) and ZO-1 (white). Scale bar, 50 μm.

(D) Quantification of the mean apical area per cell in μm^2. Data represent mean of medians ± SEM. Statistical significance was analyzed using an ANOVA test followed by Tukey's a posteriori test. *$p < 0.05$, $n = 3$ independent experiments.

(E and F) Immunostaining of NPCs for SOX1 and ZO-1 showing that NPCs exhibit different apical domain sizes in response to different LPA concentrations. (E) y-x images represent top view and z-x images side view. Scale bars, 10 μm (E) and 100 μm (F).

(G) Quantification of cellular apical domain size in μm^2. ANOVA test followed by Tukey's a posteriori test. Data represent mean of medians ± SEM. *$p < 0.05$, $n = 3$ independent experiments.

Nuclei were stained with Hoechst 33342. See also Figure S4.

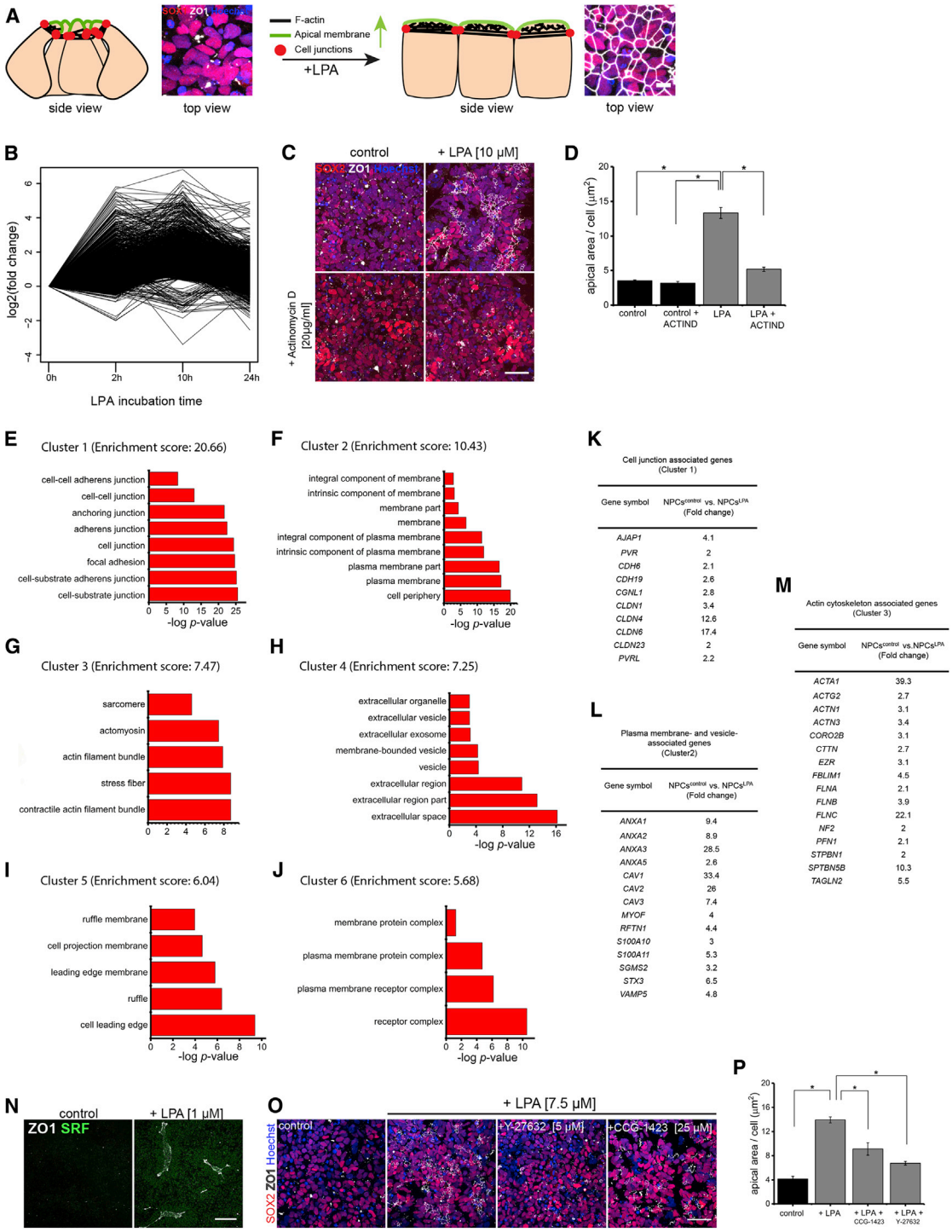

Figure 4. LPA Upregulates Genes Involved in Cell Junction, Actin Cytoskeleton, and Plasma Membrane Organization in Human NPCs

(A) Scheme illustrating potential important cellular processes involved in apical expansion of epithelial cells. Immunostaining depicts the small rosette state (left) and the large apical domain morphology of NPCs (right). Scale bar, 10 µm.

(B) Microarray analysis of control NPCs versus LPA-treated NPCs at 2 hr, 10 hr, and 24 hr after initial LPA administration. Graph depicts expression levels of all genes that show at least an upregulation of more than 2-fold in at least one of the three time points (log_2 scale).

(legend continued on next page)

state can be shortened or extended by simply incubating the cells with lower or higher LPA concentrations, as demonstrated in Figure S4.

Apical Domain Widening of Human NPCs in Response to LPA Is Transcription Dependent

Apical expansion and the arrangement of epithelial cells into a large and connected cell layer would be expected to result from increased lipid incorporation into the plasma membrane, growth and stabilization of the underlying actin cortex, and remodeling of cell junctions (Figure 4A) (Luschnig and Uv, 2014; Yeaman et al., 2004). To understand the molecular changes associated with apical domain widening of NPCs, we performed a microarray analysis whereby we compared the gene expression of small rosette NPCs versus LPA-treated large rosette NPCs at 2 hr, 10 hr, and 24 hr after initial exposure to LPA. Examination of all genes that showed an upregulation of at least 2-fold in one of the three time points revealed that most upregulation occurs at 10 hr and reverts to normal gene expression levels at 24 hr, probably due to decreasing LPA activity within the medium (Figure 4B). We wondered whether the strong induction of gene expression in the first 10 hr was crucial for apical domain widening, so we exposed NPCs to LPA and actinomycin D (ACTIND), a small molecule commonly used to block RNA synthesis. NPCs treated with LPA and ACTIND maintained a small rosette morphology that was not significantly different from control NPCs or control NPCs treated with ACTIND (Figures 4C and 4D).

LPA Upregulates Genes Involved in Apical Membrane, Cell Cortex, and Tight-Junction Function in Human NPCs

We used DAVID Bioinformatics software to identify cellular component gene ontology terms (GO_CC terms) enriched with genes that were up- or downregulated more than 2-fold in the microarray, respectively. We then performed a functional annotation clustering of the GO terms. Ordering of clusters according to their overall p value revealed that the top clusters were highly enriched in genes related to cell junction formation (cluster 1), plasma membrane (cluster 2), actin filament assembly (cluster 3), membrane-vesicle interactions (cluster 4), membrane movement and cell migration (cluster 5), and plasma membrane-receptor interactions (cluster 6) (Figures 4E–4J). Among the upregulated genes that were enriched in the six top GO clusters we found many genes related to the functions required to generate apical membrane, including actin-filament assembly-, cell junction-, plasma membrane-, and vesicle-associated genes. RNA expression levels of genes encoding for tight-junction-associated proteins of the claudin family (CLDN1, 4, 6, 23) were strongly upregulated (Furuse, 2010) (Figure 4K). Furthermore, RNA expression levels of genes that are translated into caveolins 1–3 (CAV1–3), which are involved in trafficking cholesterol-rich membranes that are enriched in the apical and basolateral surface, were highly induced, as well as the expression of other genes involved in apical vesicle trafficking and fusion, such as syntaxin 3 (*STX3*) and annexin A2 (*ANXA2*) (Martin-Belmonte et al., 2007; Scheiffele et al., 1998; Sharma et al., 2006) (Figure 4L). The apical surface is also characterized by a strong accumulation of cortical actin and correspondingly, a strong upregulation of actin (*ACTA1*) and actin-organizing and -stabilizing genes, such as profilin 1 (*PFN1*), actinin alpha 1 (*ACTN1*), cortactin (*NF2*), ezrin (*EZR*), and spectrin β5 (*SPTBN5*) could be detected (Liem, 2016; Saarikangas et al., 2010) (Figure 4M). GO analysis of genes that were downregulated by LPA (>2-fold) mainly resulted in GO clusters related to

(C) Immunostaining of NPCs for ZO-1 and SOX2 that were cultured without LPA, with LPA, or in the presence of LPA and actinomycin D (Sigma-Aldrich, cat. no. A9415). Scale bar, 50 μm.
(D) Quantification of the mean apical area per cell in μm^2.
(E–J) Functional annotation clustering of all genes upregulated more than 2-fold at 10 hr after LPA administration. The six top GO clusters exhibiting the lowest p value and highest enrichment of upregulated genes from the microarray are depicted. Clustering was performed using DAVID software. Cluster 1 = cell junction formation (E), Cluster 2 = plasma membrane (F), Cluster 3 = actin filament assembly (G), Cluster 4 = membrane-vesicle interactions (H), Cluster 5 = membrane movement and cell migration (I), Cluster 6 = plasma membrane-receptor interactions (J).
(K–M) Tables showing strongly upregulated genes (>2-fold) in response to LPA, which are associated with cell junction (K), plasma membrane (L), and actin cytoskeleton (M) organization.
(N) Immunostaining of NPCs for ZO-1 and SRF showing the upregulation of SRF in response to LPA. Scale bar, 100 μm.
(O) Immunostaining of NPCs for SOX1 and ZO-1 showing the involvement of ROCK and SRF in apical expansion of NPCs. Y-27632, ROCK inhibitor (Tocris, cat. no. 1254); CCG-1423, inhibitor of SRF-associated gene transcription (Sigma-Aldrich, cat. No. SML0987). Scale bar, 50 μm.
(P) Quantification of the apical area per cell in μm^2.
Statistical significance in (D) and (P) was analyzed using an ANOVA test followed by Tukey's a posteriori test. *$p < 0.05$, $n = 3$ independent experiments. Data represent mean of medians ± SEM. All nuclei were stained with Hoechst 33342. See also Figures S5A and S5B.

projections, axons, synapses, and calcium channels of neurons, indicating a bias in affected cellular components between the up- and downregulated genes (Tables S1 and S2).

Rho/SRF Signaling Is Involved in the Formation of a Larger Neuroepithelial-like Morphology of Human NPCs

LPA has been shown to exert many of its various cytoskeletal effects by activation of the Rho signaling pathway and the downstream transcription factor SRF, which are major regulators of actin dynamics (Hurst et al., 2008; Miano et al., 2007). We next investigated whether Rho/SRF signaling controls apical expansion and the adoption of a larger neuroepithelial-like morphology in NPCs. Immunostaining for SRF revealed a much stronger signal in LPA-treated NPCs than in control NPCs, indicating that SRF is upregulated in the presence of LPA (Figure 4N). We next tested CCG-1423, an inhibitor of SRF-driven gene expression, and Y-27632, an inhibitor of the Rho downstream kinase ROCK, on NPCs exposed to LPA. Application of both inhibitors in addition to LPA resulted in a strongly disrupted ZO-1 expression pattern compared with NPCs that were treated with LPA alone (Figure 4O). Quantification of the apical area confirmed a significant decrease per cell from 13. ± 0.5 μm^2 in the LPA-treated NPCs toward 9 ± 1 μm^2, 6.8 ± 0.3 μm^2, and 4.2 ± 0.4 μm^2 apical area in NPCs that were additionally incubated with CCG-1423, with Y-27632, or without LPA (control), respectively (Figure 4P). LPA also activates Ca^{2+}-dependent signaling pathways in NPCs of the developing brain that influence many cellular processes (Dubin et al., 2010). To test the importance of calcium signaling in apical expansion, we applied the inhibitors edelfosine (blockage of phospholipase C), 2-APB (blockage of inositol triphosphate receptors), BAPTA-AM (depletion of intracellular Ca^{2+} levels), and EGTA (depletion of extracellular Ca^{2+} levels) to NPCs in the presence of LPA. The quantification of the apical area showed that exposure to 2-APB and edelfosine resulted in significantly decreased apical areas within the 5 hr of incubation time, where no toxic effects of the inhibitors were observed at the concentrations we employed (Figures S5A and S5B).

Maintenance of Apical Domain-Forming Capacity in Human NPCs over 52 Passages

We next investigated whether NPCs maintained their inducibility by LPA at different passage numbers. Under normal culture conditions, NPCs at RP1 or RP2 formed very large rosettes in response to LPA. However, at RP3 the ability of the cells to adopt a large rosette morphology decreased and at RP4 the cells did no longer formed large rosettes in response to a 1-day pulse-treatment of LPA (Figure 5A). Based on these results, we tested whether a continuous exposure of NPCs to LPA could maintain the competence to form large rosettes. We cultured NPCs from RP1 with a continuous exposure to 1–2 μM LPA (see Supplemental Experimental Procedures). Continuous exposure to this level of LPA yielded $SOX2^+$ cultures with strongly expanded cellular apical domains and a large rosette morphology. The maintenance of apical domain expansion was preserved over 52 passages (Figures 5B and S5C).

LPA Prevents Neuronal and Glial Differentiation in Early-Stage and Long-Term LPA-Treated Human NPCs

We further tested whether the maintenance of a large apical domain NPC phenotype yielded reduced neuronal and glial differentiation of the NPC cultures. We exposed NPCs for 3 days to constant levels of 0.5 μM LPA (see Supplemental Experimental Procedures) and investigated the neuronal differentiation rates. Compared with control small rosette NPCs, the cells supplied with LPA exhibited broad apical domains with an even ZO-1 distribution (Figure 5C, upper panels). Immunostaining for the neuronal markers TUBB3 and HuC/HuD and quantification of HuC/HuD^+ cells revealed that 3.9% ± 0.5% of the cells from the control expressed HuC/HuD, whereas 0.9% ± 0.2% of the LPA-treated NPCs showed expression (Figures 5C [middle panels], 5D, and S5D). LPA has been reported to increase apoptosis in hESC-derived neurospheres (Frisca et al., 2013). To exclude the possibility that the reduced neuronal differentiation rates were a consequence of an LPA-stimulated increase in apoptosis in the developing neurons, we determined the percentage of HuC/HuD^+ cells that co-expressed the apoptotic marker caspase-3 (CASP3). Quantification of the $HuC/HuD^+/CASP3^+$ cells did not reveal a significant difference in the apoptotic rates between control NPCs and LPA-treated NPCs (Figures 5C [middle panels] and 5E). We next assessed whether LPA exposure also prevents the transformation of NPCs toward a radial glial phenotype. Control cells cultured for 22 passages displayed high levels of glial fibrillary acidic protein (GFAP) immunofluorescence signal while NPCs cultured for 22 passages in medium continuously supplemented with LPA (see Supplemental Experimental Procedures) had a markedly reduced GFAP immunofluorescence intensity, representing a 92% decreased signal (Figures 5C [lower panels] and 5F). Finally, we asked whether NPC cells that had been cultured long term in LPA retain their neuronal differentiation potential. LPA-treated RP14 NPC cultures were deprived of LPA for 5 days and examined for markers of neuronal differentiation. 19% ± 1% of cells expressed HuC/HuD and had mean $TUBB3^+$ areas of 47 ± 5 μm^2 per cell, values that were in the range of non-LPA-treated

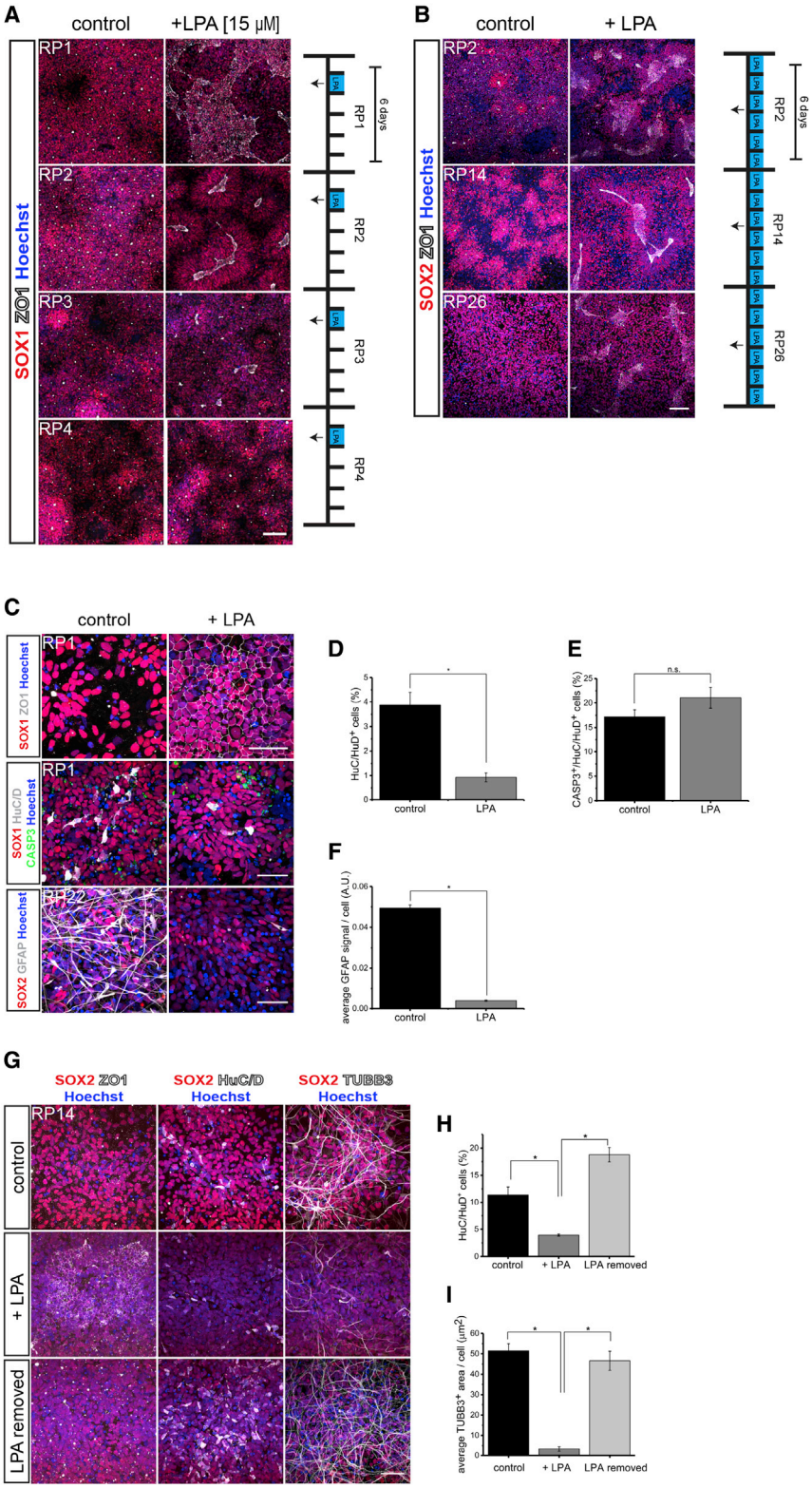

Figure 5. Constant LPA Exposure Maintains the Large Rosette Formation Capacity of Human NPCs

(A) Immunostaining of untreated or LPA-treated NPCs at different passaging numbers for SOX1 and ZO-1. Contrast for ZO-1 signal is enhanced in upper left image. Scale bar, 100 μm.

(B) NPCs that have constantly been cultured without or with LPA for 26 passages show different rosette sizes. Immunofluorescence of NPCs for SOX1 (red) and ZO-1 (white). Scale bar, 100 μm.

(C) LPA prevents neuronal and glial differentiation without an increase in apoptosis. Immunostaining of NPCs for SOX1 (red), SOX2 (red), ZO-1 (white), HuC/HuD (white), GFAP (white), and CASP3 (green). Scale bars, 50 μm.

(D) Quantification of the percentage of HuC^+/HuD^+ cells.

(E) Quantification of $HuC^+/HuD^+/CASP3^+$ double-positive cells.

(F) Quantification of the average GFAP intensity (a.u.) per cell.

(G) LPA exposure does not impair differentiation potential of NPCs. Cells passaged for 14 passages in LPA were either maintained in LPA (+LPA) or deprived of LPA for 5 days (LPA removed) and assayed for neural differentiation. Immunostaining of NPCs for SOX2 (red), TUBB3 (white), HuC/HuD (white), and ZO-1 (white). Scale bar, 50 μm.

(H and I) Quantification of the percentage of HuC^+/HuD^+ cells (H) and the mean $TUBB3^+$ area per cell in μm^2 (I).

For (D), (E), (F), (H), and (I), statistical significance was analyzed using a t test. *$p < 0.05$, $n = 3$ independent experiments. Data represent mean of medians ± SEM. Nuclei were stained with Hoechst 33342. See also Figures S5C and S5D.

cells (HuC/HuD, 11% ± 1%; TUBB3$^+$ area/cell, 51 ± 4 μm^2) and higher than cells that had been continuously exposed to LPA (HuC/HuD, 3.9% ± 0.2%; TUBB3$^+$ area/cell, 3 ± 1 μm^2) (Figures 5G–5I). These results indicate that propagation of rosette-forming neuroepithelia using LPA does not compromise their differentiation potential compared with controls.

DISCUSSION

Rosette-forming NPCs are considered to represent a very early-stage NSC type that can differentiate into diverse neuronal and glial subtypes (Broccoli et al., 2014; Kriks et al., 2011). Unfortunately the rosette state could not previously be maintained for many passages. So far only few factors, such as SHH and Notch signaling agonists, have been identified that are able to maintain a rosette phenotype in cultured NPCs for up to four passages presumably by promoting self-renewing cell divisions. In addition, Koch et al. developed a protocol whereby NPCs could be passaged for >150 passages in the presence of fibroblast growth factor 2 (FGF2) and epidermal growth factor (EGF) without losing a small rosette phenotype and neuronal differentiation potential (Elkabetz et al., 2008; Koch et al., 2009). Here we identify LPA as a serum factor that has a major effect on the expansion of the apical membrane of cultured axolotl and human NPCs, resulting in the formation of very large rosette structures, which in the case of human NPCs can be maintained for at least 52 passages if constantly supplied with LPA. Large rosette formation of human NPCs occurs irrespective of cell proliferation but is rather a consequence of apical domain expansion and concomitant with the opening up of existing small rosettes and their fusion into larger epithelial cell clusters. The long-term LPA-treated human NPCs are competent in undergoing neuronal and glial differentiation once LPA is withdrawn from the medium. In former publications LPA has been shown to prevent neuronal, but not glial, differentiation of hESC- and iPSC-derived plated neurospheres (Dottori et al., 2008; Frisca et al., 2013). Using our protocol we show that long-term LPA exposure prevents both neuronal and glial differentiation in NPCs. The opposing results could be due to differences in the culturing protocols and the timing of LPA treatment. In the future it will be interesting to assess whether long-term LPA-cultured NPCs can also yield differently patterned neuronal subtypes.

Another very interesting phenotype is the LPA-mediated expansion of the apical domain of NPCs itself. Few molecules have been shown to regulate apical domain size in epithelial cells. Deregulation of components of the Hippo signaling pathway, such as knockdown of the scaffolding protein KIBRA or expression of the CDC42 activator DBL3, can lead to apical expansion in MDCK cells. Also, overexpression of the protein Crumbs resulted in an apical expansion of *Drosophila* embryonic epithelia (Wodarz et al., 1995; Yoshihama et al., 2011; Zihni et al., 2014). In our microarray we could not detect significant changes in the expression levels of the involved Hippo signaling components or Crumbs, implying that apical expansion in NPCs might be mediated by a different mechanism. Indeed, we could identify top GO term clusters and strongly induced genes related to cell junction-, actin-, and plasma membrane-related cellular processes, which have been described as important processes during the luminogenesis of epithelial tissues (Datta et al., 2011; Luschnig and Uv, 2014). In the future, knockout studies will need to be performed to identify the key genes that promote apical expansion.

Binding of LPA to most of its receptors activates the Rho signaling pathway and the associated downstream factors ROCK1 and SRF (Hurst et al., 2008; Miano et al., 2007). In our experiments we also observed a strong dependency of large apical domain formation on ROCK1 and SRF. A literature-based metacore analysis of all SRF target genes revealed a total of 439 binding targets, among which 105 target genes were found to be up- or downregulated (>2-fold) in our microarray data, while most of the upregulated genes were found to be transcriptional activators (Table S3 and Figure S5E). The fact that around 25% of all SRF target genes exhibited differential gene expression in response to LPA suggests an important role for SRF in mediating apical expansion. In addition, we do not exclude that activation of the Ca^{2+} signaling pathway by LPA plays an important role in conveying apical expansion, since blockage of phospholipase C and IP3R Ca^{2+} channels by pharmacological inhibitors could also reduce apical expansion. Both signaling pathways could act in combination to promote expansion of the apical domain.

Kingsbury et al. (2003) observed the formation of gyri and an increased cortical thickness when they cultured E14 brain sections of the mouse telencephalon in an *in vitro* slice culture system in the presence of LPA. Growth in cortical size was attributed to a larger NPC pool and increased terminal neuronal cell divisions. However, those phenotypes could hardly explain gyri formation, and it was suggested that other LPA-initiated signaling pathways might cause the folding. In our system we can also observe the formation of a large pseudostratified rosette neuroepithelium, which also contains strongly folded regions that resemble gyri. In this regard it is tempting to speculate whether an expansion of the apical domain of the NPCs close to the VZ could increase the total apical surface of the VZ, which could lead to more apical tension or a rearrangement of cells and provide a stimulus for the folding.

Hence it would be interesting to find out whether folding of mouse brain cortices in the presence of ROCK or SRF inhibitor would be impaired.

During development, many future lumen-containing epithelial tissues, such as pancreatic or kidney tissue, form rosettes as intermediate structures during lumen morphogenesis. The rosettes then fuse with each other to create larger tubular structures (Harding et al., 2014). As LPA promotes the fusion of adjacent small rosettes into larger luminal structures in our system, it will also be tempting to test whether LPA can promote the organization of other rosette-forming epithelial tissues into larger luminal structures.

EXPERIMENTAL PROCEDURES

Axolotl NSC Culture

Axolotl spinal cord explants were dissociated into single cells using PBS/EDTA and plated on 12-well plates coated with gelatin at a density of 32,000 cells/cm^2. Cells were passaged every 3 weeks and cultured in DMEM/F-12 medium supplemented with human FGF2 and B27 (Gibco). For large rosette induction, the culture medium was supplemented for 3 days with either 30% fetal bovine serum or 20–50 μM LPA 1 day after passaging with a daily medium change. After 3 days of serum or LPA treatment, cells were cultured for another 25 days in normal culturing medium to allow for large rosette formation.

hESC Culture and Neural Differentiation

For hESC culture, the hESC lines H9 and H1 were used (WA09, WA01; WiCell). hESCs were cultured as described previously (Zhu et al., 2013). Neural differentiation was performed according to a modified version of published protocols (Khattak et al., 2015). hESC clumps were cultured for 5 days in low-attachment well plates in the presence of mTeSR1 medium (STEMCELL Technologies), supplemented with 2 μM dorsomorphin (Sigma-Aldrich, cat. no. 5499) and 10 μM SB431542 (Tocris, cat. no. 1614). Under floating conditions the cell clumps formed embryoid bodies (EBs). After 5 days the EBs were transferred to well plates coated with growth factor reduced Matrigel (GFRM; Corning) and cultured in the presence of the same medium. After 7 days rosettes had formed, which were dissociated with Dulbecco's PBS (without $MgCl_2$, $CaCl_2$)/0.1 mM EDTA into single cells and plated at a density of 450,000 cells/cm^2 on well plates coated with GFRM. Medium was changed to N2B27 medium (Zhu et al., 2013) supplemented with human FGF2 (20 ng/mL) and mouse EGF (10 ng/mL). NPCs were passaged every 6 days (RP = rosette passaging number, which indicates how often the cells have been passaged; see also Figure S1). For Figure 1A (lower panels) NPCs were obtained using a three-dimensional cyst-based neural differentiation protocol published previously (Zhu et al., 2013).

Immunostaining and Microscopy

NPCs were fixed in 4% paraformaldehyde in plastic- or glass-bottom 24-well plates and immunostained as described previously (Zhu et al., 2013). Cells were imaged using the confocal microscopes Zeiss LSM 700, LSM 710, LSM 780, and LSM 880 (10×, 20×, 40×, and 63× objective) and the Leica DMI 4000 B (63× objective). Confocal images are either single-stack images or z stack images where maximum-intensity projection was performed. Phase-contrast images were obtained using the Leica DM IL. Images were processed using ImageJ, Photoshop, and Illustrator software. A full list with all primary and secondary antibodies is provided in Supplemental Experimental Procedures.

Statistics and Image Analysis

Image analysis was performed by using Cell Profiler and Fiji software. For each experimental condition tested at least three independent experiments were analyzed. From each replicate either the number of rosettes per image (Figure 1G), the distribution of apical rosette area (Figure 1E), number of SOX1$^+$ cells participating in rosette formation (Figure 1F), and the cellular apical domain size (Figure 3G) were determined. Since the data were non-normally distributed, the median for each replicate was determined, upon which the mean and the SEM for each experimental condition was calculated. For all other quantifications, mean and SEM were determined. After checking the homogeneity of variances by the Brown-Forsythe test, statistical comparisons were performed by a t test or ANOVA test followed by Tukey's a posteriori test when comparing two conditions or more than two conditions, respectively.

ACCESSION NUMBERS

The accession number for the microarray data reported in this paper is GEO: GSE111597.

SUPPLEMENTAL INFORMATION

Supplemental Information includes Supplemental Experimental Procedures, five figures, and three tables and can be found with this article online at https://doi.org/10.1016/j.stemcr.2018.04.018.

AUTHOR CONTRIBUTIONS

J.-P.M., L.M., and E.M.T. conceived the project and conceptualized the experiments. J.-P.M. performed all experiments with hESC-derived NPCs and acquired, analyzed, and interpreted the data. L.M. and K.R. performed all the experiments with axolotl NPCs and acquired, analyzed, and interpreted the data. O.C., S.O., and A.d.S. analyzed and interpreted the data. O.C. performed statistical analysis and revised the manuscript. J.-P.M. and E.M.T. wrote the manuscript.

ACKNOWLEDGMENTS

We thank T. Lendl and P. Pasierbek from the IMP Biooptics Facility for help with imaging and image analysis. We also thank S. Khattak from the CRTD/TU Dresden ES/iPS Cell Facility for advice with neuronal differentiation. Furthermore, we thank K. Goehler and R. Wegner for technical assistance. We are also grateful to Julia Jarrells from the MPI-CBG Microarray DNA Facility/Dresden for expert advice and assistance. This work was supported by grants

from the DFG, FZ-111, EXC168, and SFB655 From Cells into Tissues to E.M.T. O.C. is a career researcher from Consejo Nacional de Investigaciones Científicas y Técnicas (CONICET) of Argentina and was supported by a grant from Agencia Nacional de Promoción Científica y Tecnológica (ANPCyT) PICT-2014-3469. S.O. is supported by an FNR CORE grant (C15/BM/10397420).

Received: October 2, 2017
Revised: April 20, 2018
Accepted: April 20, 2018
Published: May 17, 2018

REFERENCES

Aaku-Saraste, E., Hellwig, A., and Huttner, W.B. (1996). Loss of occludin and functional tight junctions, but not ZO-1, during neural tube closure-remodeling of the neuroepithelium prior to neurogenesis. Dev. Biol. *180*, 664–679.

Broccoli, V., Giannelli, S.G., and Mazzara, P.G. (2014). Modeling physiological and pathological human neurogenesis in the dish. Front. Neurosci. *8*, 183.

Chambers, S.M., Fasano, C.A., Papapetrou, E.P., Tomishima, M., Sadelain, M., and Studer, L. (2009). Highly efficient neural conversion of human ES and iPS cells by dual inhibition of SMAD signaling. Nat. Biotechnol. *27*, 275–280.

Currie, J.D., Kawaguchi, A., Traspas, R.M., Schuez, M., Chara, O., and Tanaka, E.M. (2016). Live imaging of axolotl digit regeneration reveals spatiotemporal choreography of diverse connective tissue progenitor pools. Dev. Cell *39*, 411–423.

Datta, A., Bryant, D.M., and Mostov, K.E. (2011). Molecular regulation of lumen morphogenesis. Curr. Biol. *21*, R126–R136.

Dottori, M., Leung, J., Turnley, A.M., and Pebay, A. (2008). Lysophosphatidic acid inhibits neuronal differentiation of neural stem/progenitor cells derived from human embryonic stem cells. Stem Cells *26*, 1146–1154.

Dubin, A.E., Herr, D.R., and Chun, J. (2010). Diversity of lysophosphatidic acid receptor-mediated intracellular calcium signaling in early cortical neurogenesis. J. Neurosci. *30*, 7300–7309.

Eiraku, M., Takata, N., Ishibashi, H., Kawada, M., Sakakura, E., Okuda, S., Sekiguchi, K., Adachi, T., and Sasai, Y. (2011). Self-organizing optic-cup morphogenesis in three-dimensional culture. Nature *472*, 51–56.

Elkabetz, Y., Panagiotakos, G., Al Shamy, G., Socci, N.D., Tabar, V., and Studer, L. (2008). Human ES cell-derived neural rosettes reveal a functionally distinct early neural stem cell stage. Genes Dev. *22*, 152–165.

Frisca, F., Crombie, D.E., Dottori, M., Goldshmit, Y., and Pebay, A. (2013). Rho/ROCK pathway is essential to the expansion, differentiation, and morphological rearrangements of human neural stem/progenitor cells induced by lysophosphatidic acid. J. Lipid Res. *54*, 1192–1206.

Furuse, M. (2010). Molecular basis of the core structure of tight junctions. Cold Spring Harb. Perspect. Biol. *2*, a002907.

Harding, M.J., McGraw, H.F., and Nechiporuk, A. (2014). The roles and regulation of multicellular rosette structures during morphogenesis. Development *141*, 2549–2558.

Hurst, J.H., Mumaw, J., Machacek, D.W., Sturkie, C., Callihan, P., Stice, S.L., and Hooks, S.B. (2008). Human neural progenitors express functional lysophospholipid receptors that regulate cell growth and morphology. BMC Neurosci. *9*, 118.

Khattak, S., Brimble, E., Zhang, W., Zaslavsky, K., Strong, E., Ross, P.J., Hendry, J., Mital, S., Salter, M.W., Osborne, L.R., et al. (2015). Human induced pluripotent stem cell derived neurons as a model for Williams-Beuren syndrome. Mol. Brain *8*, 77.

Kingsbury, M.A., Rehen, S.K., Contos, J.J., Higgins, C.M., and Chun, J. (2003). Non-proliferative effects of lysophosphatidic acid enhance cortical growth and folding. Nat. Neurosci. *6*, 1292–1299.

Koch, P., Opitz, T., Steinbeck, J.A., Ladewig, J., and Brustle, O. (2009). A rosette-type, self-renewing human ES cell-derived neural stem cell with potential for in vitro instruction and synaptic integration. Proc. Natl. Acad. Sci. USA *106*, 3225–3230.

Kriks, S., Shim, J.W., Piao, J., Ganat, Y.M., Wakeman, D.R., Xie, Z., Carrillo-Reid, L., Auyeung, G., Antonacci, C., Buch, A., et al. (2011). Dopamine neurons derived from human ES cells efficiently engraft in animal models of Parkinson's disease. Nature *480*, 547–551.

Li, X.J., Du, Z.W., Zarnowska, E.D., Pankratz, M., Hansen, L.O., Pearce, R.A., and Zhang, S.C. (2005). Specification of motoneurons from human embryonic stem cells. Nat. Biotechnol. *23*, 215–221.

Liem, R.K. (2016). Cytoskeletal integrators: the spectrin superfamily. Cold Spring Harb. Perspect. Biol. *8*. https://doi.org/10.1101/cshperspect.a018259.

Luschnig, S., and Uv, A. (2014). Luminal matrices: an inside view on organ morphogenesis. Exp. Cell Res. *321*, 64–70.

Martin-Belmonte, F., Gassama, A., Datta, A., Yu, W., Rescher, U., Gerke, V., and Mostov, K. (2007). PTEN-mediated apical segregation of phosphoinositides controls epithelial morphogenesis through Cdc42. Cell *128*, 383–397.

Meinhardt, A., Eberle, D., Tazaki, A., Ranga, A., Niesche, M., Wilsch-Brauninger, M., Stec, A., Schackert, G., Lutolf, M., and Tanaka, E.M. (2014). 3D reconstitution of the patterned neural tube from embryonic stem cells. Stem Cell Reports *3*, 987–999.

Miano, J.M., Long, X., and Fujiwara, K. (2007). Serum response factor: master regulator of the actin cytoskeleton and contractile apparatus. Am. J. Physiol. Cell Physiol. *292*, C70–C81.

Pebay, A., Bonder, C.S., and Pitson, S.M. (2007). Stem cell regulation by lysophospholipids. Prostaglandins Other Lipid Mediat. *84*, 83–97.

Rodrigo Albors, A., Tazaki, A., Rost, F., Nowoshilow, S., Chara, O., and Tanaka, E.M. (2015). Planar cell polarity-mediated induction of neural stem cell expansion during axolotl spinal cord regeneration. eLife *4*, e10230.

Rost, F., Albors, A.R., Mazurov, V., Brusch, L., Deutsch, A., Tanaka, E.M., and Chara, O. (2016). Accelerated cell divisions drive the outgrowth of the regenerating spinal cord in axolotls. eLife *5*, e20357.

Saarikangas, J., Zhao, H., and Lappalainen, P. (2010). Regulation of the actin cytoskeleton-plasma membrane interplay by phosphoinositides. Physiol. Rev. *90*, 259–289.

Scheiffele, P., Verkade, P., Fra, A.M., Virta, H., Simons, K., and Ikonen, E. (1998). Caveolin-1 and -2 in the exocytic pathway of MDCK cells. J. Cell Biol. *140*, 795–806.

Sharma, N., Low, S.H., Misra, S., Pallavi, B., and Weimbs, T. (2006). Apical targeting of syntaxin 3 is essential for epithelial cell polarity. J. Cell Biol. *173*, 937–948.

Wagner, I., Wang, H., Weissert, P.M., Straube, W.L., Shevchenko, A., Gentzel, M., Brito, G., Tazaki, A., Oliveira, C., Sugiura, T., et al. (2017). Serum proteases potentiate BMP-induced cell cycle re-entry of dedifferentiating muscle cells during newt limb regeneration. Dev. Cell *40*, 608–617.e6.

Walder, S., Zhang, F., and Ferretti, P. (2003). Up-regulation of neural stem cell markers suggests the occurrence of dedifferentiation in regenerating spinal cord. Dev. Genes Evol. *213*, 625–630.

Wodarz, A., Hinz, U., Engelbert, M., and Knust, E. (1995). Expression of crumbs confers apical character on plasma membrane domains of ectodermal epithelia of *Drosophila*. Cell *82*, 67–76.

Yeaman, C., Grindstaff, K.K., and Nelson, W.J. (2004). Mechanism of recruiting Sec6/8 (exocyst) complex to the apical junctional complex during polarization of epithelial cells. J. Cell Sci. *117*, 559–570.

Yoshihama, Y., Sasaki, K., Horikoshi, Y., Suzuki, A., Ohtsuka, T., Hakuno, F., Takahashi, S., Ohno, S., and Chida, K. (2011). KIBRA suppresses apical exocytosis through inhibition of aPKC kinase activity in epithelial cells. Curr. Biol. *21*, 705–711.

Yung, Y.C., Stoddard, N.C., and Chun, J. (2014). LPA receptor signaling: pharmacology, physiology, and pathophysiology. J. Lipid Res. *55*, 1192–1214.

Zhou, J., Su, P., Li, D., Tsang, S., Duan, E., and Wang, F. (2010). High-efficiency induction of neural conversion in human ESCs and human induced pluripotent stem cells with a single chemical inhibitor of transforming growth factor beta superfamily receptors. Stem Cells *28*, 1741–1750.

Zhu, Y., Carido, M., Meinhardt, A., Kurth, T., Karl, M.O., Ader, M., and Tanaka, E.M. (2013). Three-dimensional neuroepithelial culture from human embryonic stem cells and its use for quantitative conversion to retinal pigment epithelium. PLoS One *8*, e54552.

Zihni, C., Munro, P.M., Elbediwy, A., Keep, N.H., Terry, S.J., Harris, J., Balda, M.S., and Matter, K. (2014). Dbl3 drives Cdc42 signaling at the apical margin to regulate junction position and apical differentiation. J. Cell Biol. *204*, 111–127.

Stem Cell Reports, Volume *10*

Supplemental Information

Signaling-Dependent Control of Apical Membrane Size and Self-Renewal in Rosette-Stage Human Neuroepithelial Stem Cells

Jan-Philip Medelnik, Kathleen Roensch, Satoshi Okawa, Antonio del Sol, Osvaldo Chara, Levan Mchedlishvili, and Elly M. Tanaka

Supplemental Data Items

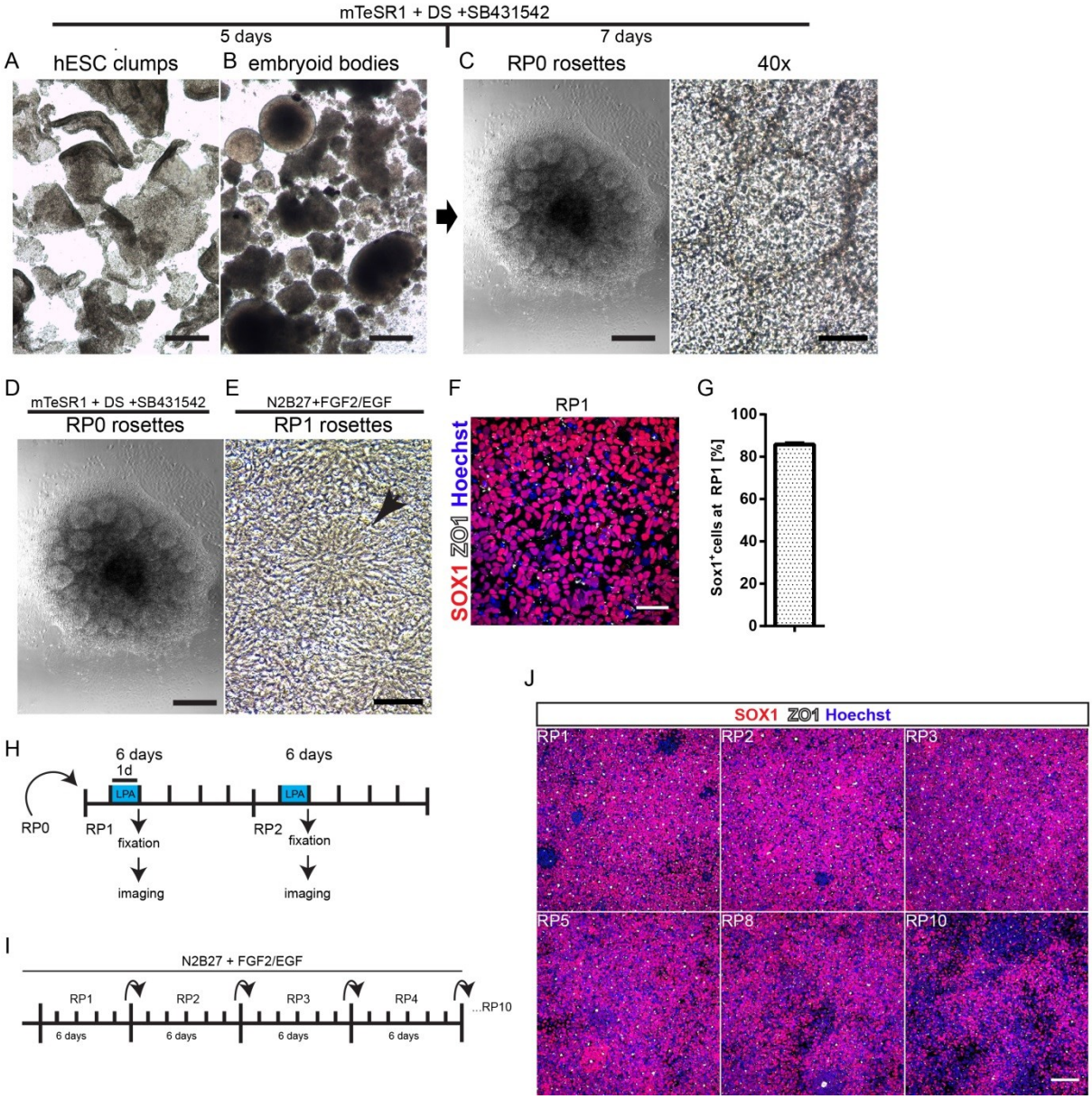

Figure S1. Three-dimensional Dual SMAD signaling inhibition protocol. Phase contrast images of cells during the neural differentiation process. **Related to Figure 1**. (A) HESC- clumps in a non-adherent cell culture dish. Scale bar is 500 µm. (B) Floating embryoid bodies (EBs). Scale bar is 500 µm. (C) Plated EBs that attached to a 6-well plate coated with growth factor reduced matrigel (GFRM, Corning). Rosette formation of EBs after 7 days of culture. RP0 rosettes, left: low magnification image. Scale bar is 500 µm. Right: high magnification image. Scale bar is 50 µm. RP0 = rosette passaging number 0, indicates that the cells have not been passaged so far. (D) Plated EBs (same image as in Fig. S1C). (E) RP0 rosette NPCs were dissociated into single cells and plated at high density. NPCs (RP1) reorganize into rosettes after passaging (see arrow). RP1 rosettes were maintained for 5 days in N2B27+FGF2/EGF medium. Scale bar is 50 µm. RP1 = rosette passaging number 1, indicates that the NPCs have been passaged once. (F) Immunostaining of RP1 NPCs two days after plating for SOX1 and ZO-1. Scale bar is 50 µm. (G) Quantification of the total number of $SOX1^+$ NPCs from the total number of cells per image. Data represent mean +/- SD, n = 3 independent experiments. DS = dorsomorphin, SB431542 = TGFbeta-signaling inhibitor, mTeSR1 = HESC- culturing medium. (H) Scheme depicting the general experimental setup for most of the experiments presented in this study. At RP0 the NPCs were passaged to RP1 or to RP2. Two days after plating LPA was added at different concentrations to the NPCs for a period of

0-24 h in 0.5 ml N2B27 + FGF2/EGF medium in 24-well plates. (I) Scheme illustrating the NPC- culturing and passaging conditions. NPCs were plated on 24-well plates coated with GFRM and cultured in 0.5 ml of N2B27 + FGF2/EGF medium. Cells were passaged every 6 days into new well plates. (J) Immunostaining of NPCs at different passaging numbers (RP1-RP10) for SOX1 and ZO-1. Nuclei in all images were labelled with Hoechst 33342. Scale bar is 100 μm. For a detailed description of the LPA assays see Supplemental Experimental Procedures.

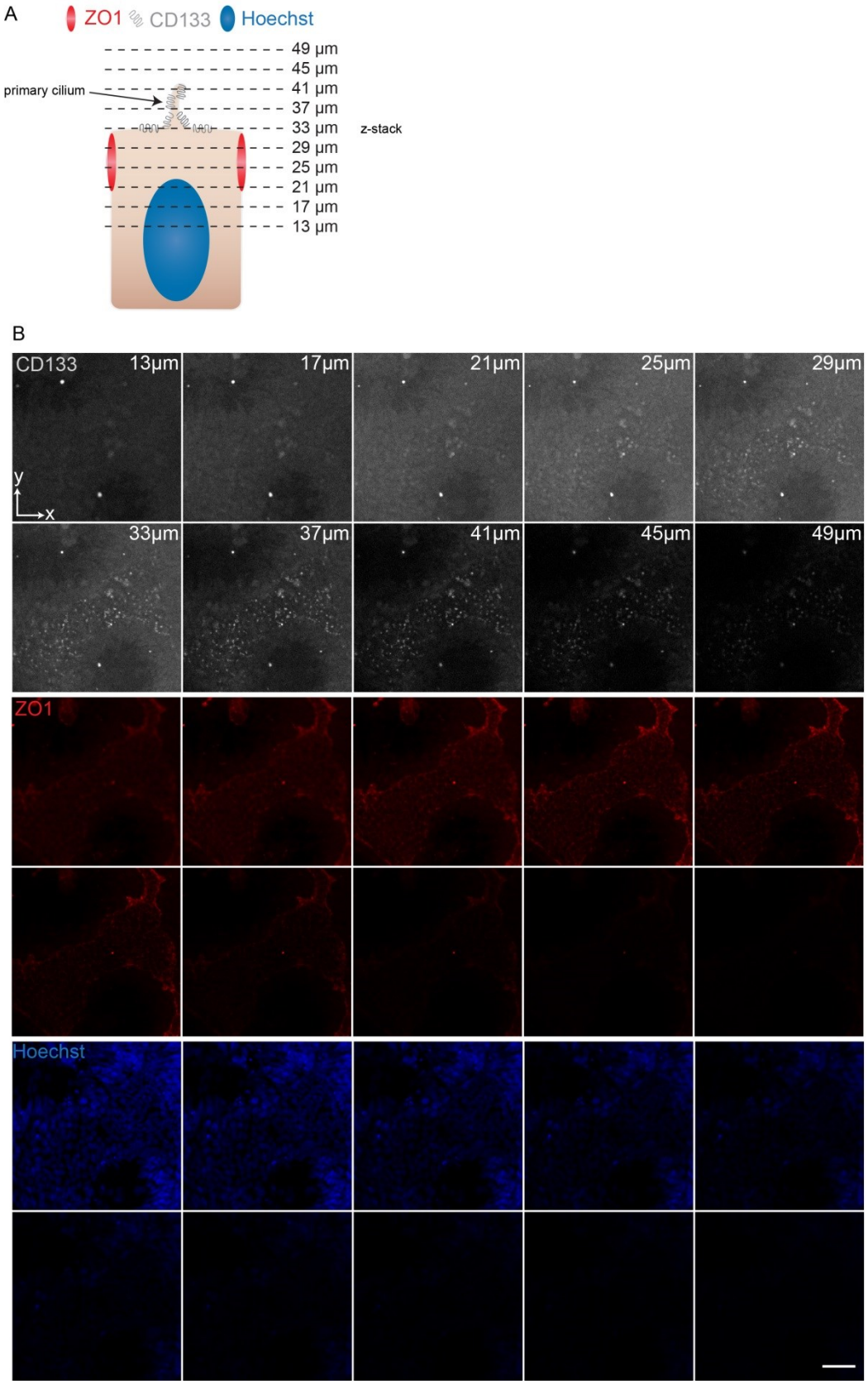

Figure S2. LPA-induced neural rosettes express CD133. **Related to Figure 1**. Z-stack images of HESC-derived NPCs incubated with 15 µM LPA for 18 h. Distances in µm indicate the distance of the respective image from the plate bottom. Immunostaining for ZO-1 and CD133 (Prominin-1). Nuclei were labelled with Hoechst 33342. Arrows indicate small dots of CD133 expression. Scale bar is 50 µm.

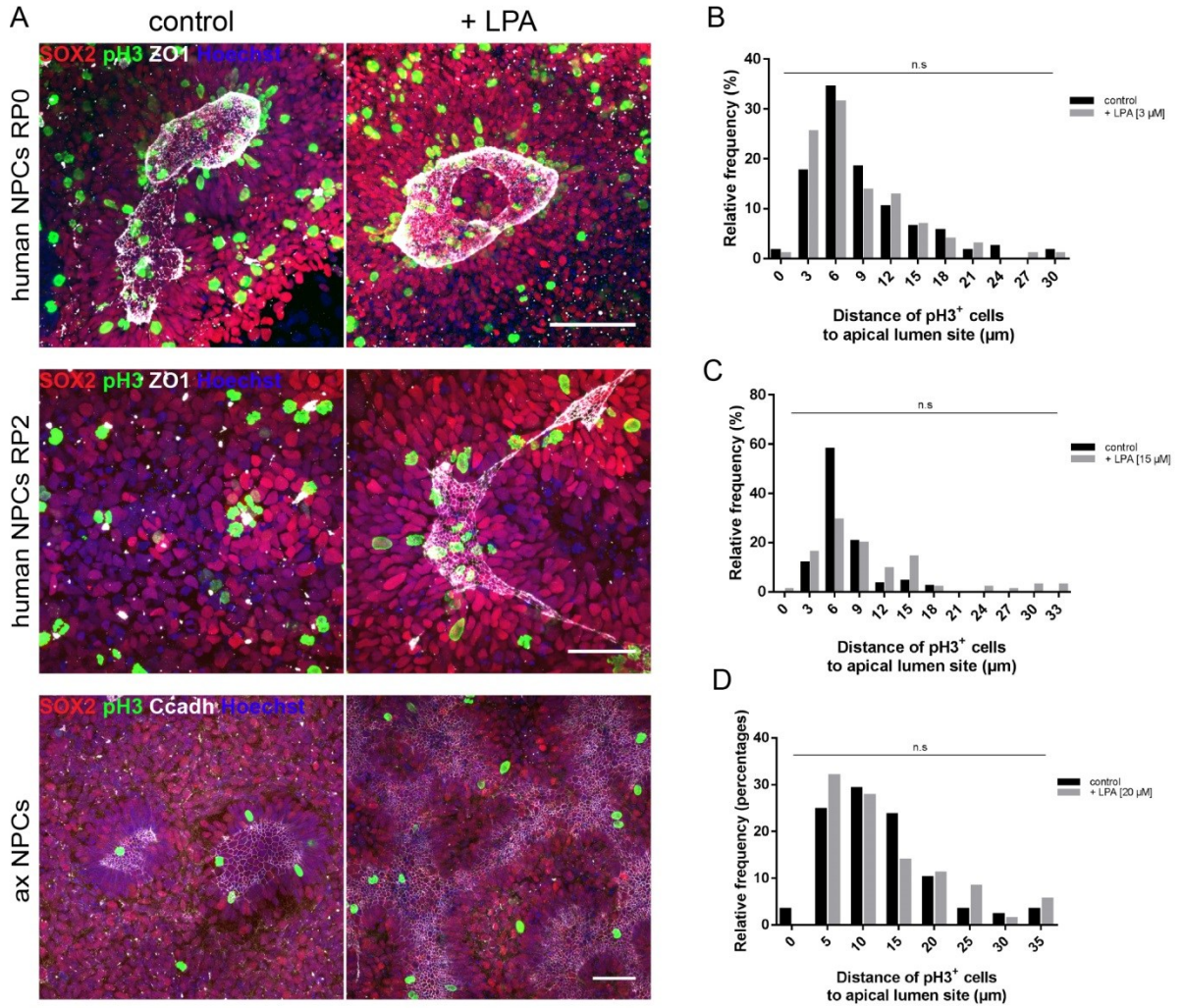

Figure S3. Position of M-phase nuclei is not altered in HESC-derived- and axolotl rosette-NPCs in the presence of LPA. **Related to Figure 2**. (A) HESC-derived NPCs at RP0 (upper panels), RP2 (middle panels) and axolotl NPCs (lower panels) were cultured in the absence (control) or presence of LPA (+ LPA) (see Supplemental Experimental Procedures). HESC-derived NPCs were immunostained for ZO-1, SOX2 and phospho-Histone H3 (pH3). Axolotl NPCs were stained for SOX2, C-cadherin and pH3. All nuclei were stained with Hoechst 33342. Scale bars are 100 µm (upper and lower panel) and 50 µm (middle panel). **(B-D)** Quantification of the relative frequencies of the distances from the center of the $pH3^+$ nuclei surrounding a lumen towards the apical lumen site in control- and LPA-treated HESC-derived and axolotl NPCs. (B-D) Relative distances of $pH3^+$ nuclei towards the lumen site of HESC-derived NPCs at RP0 (B), RP2(C) and axolotl NPCs (D). *n = 3* independent experiments. Measured distances from control and LPA-treated replicates were pooled respectively and statistical analysis was performed using a u-test.

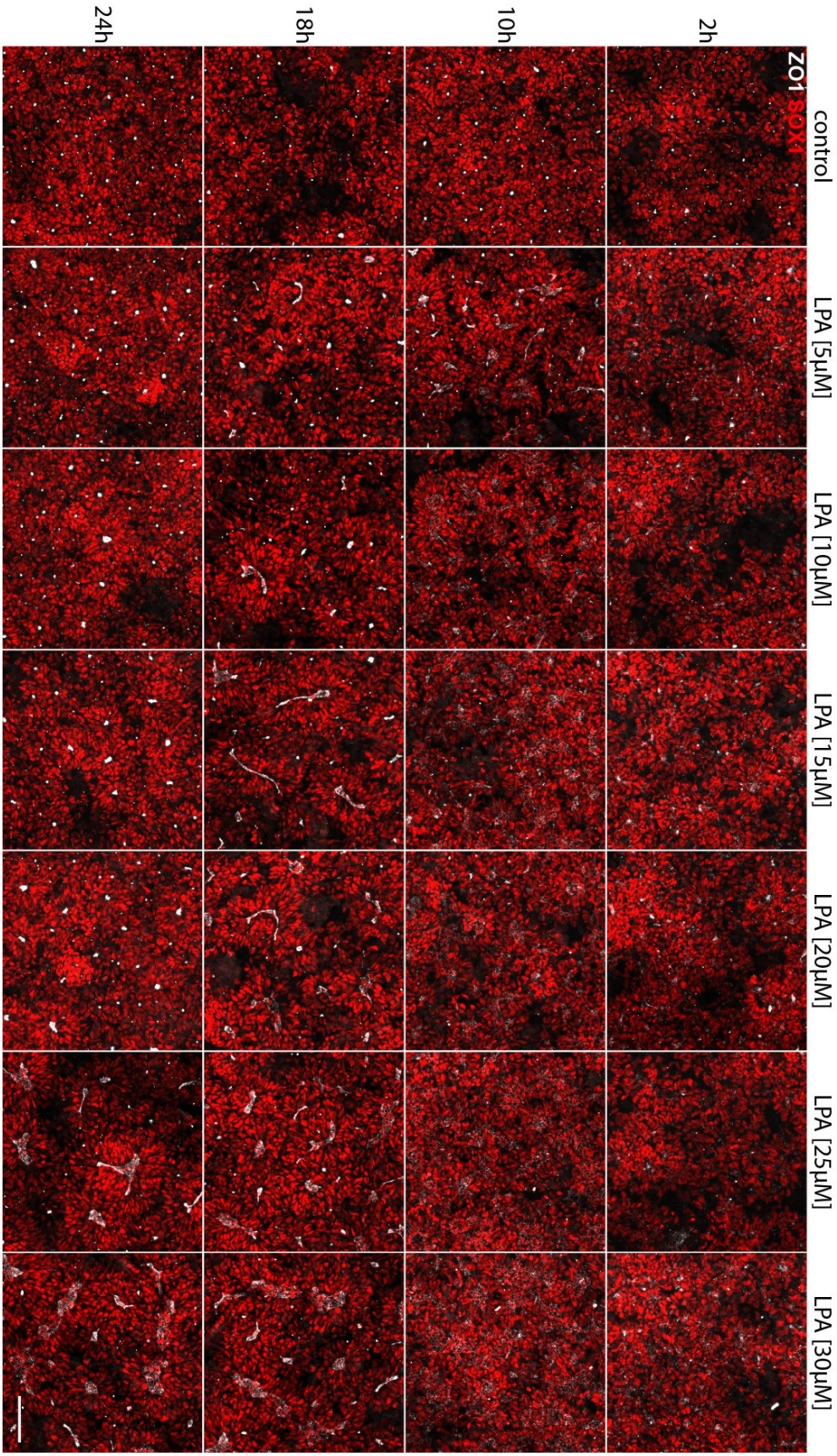

Figure S4. Time-course of the large rosette formation process of HESC-derived NPCs exposed to different LPA concentrations. **Related to Figure 3.** Immunofluorescence of NPCs that were sequentially fixed at 2 h, 10 h, 18 h and 24 h after an initial exposure to LPA concentrations ranging from 0 – 30 μM in a media volume of 0.5 ml reveals that the onset of large rosette formation can be shortened/extended by incubating the NPCs with different LPA concentrations. NPCs were stained for SOX1 and ZO1. Scale bar is 100 μm.

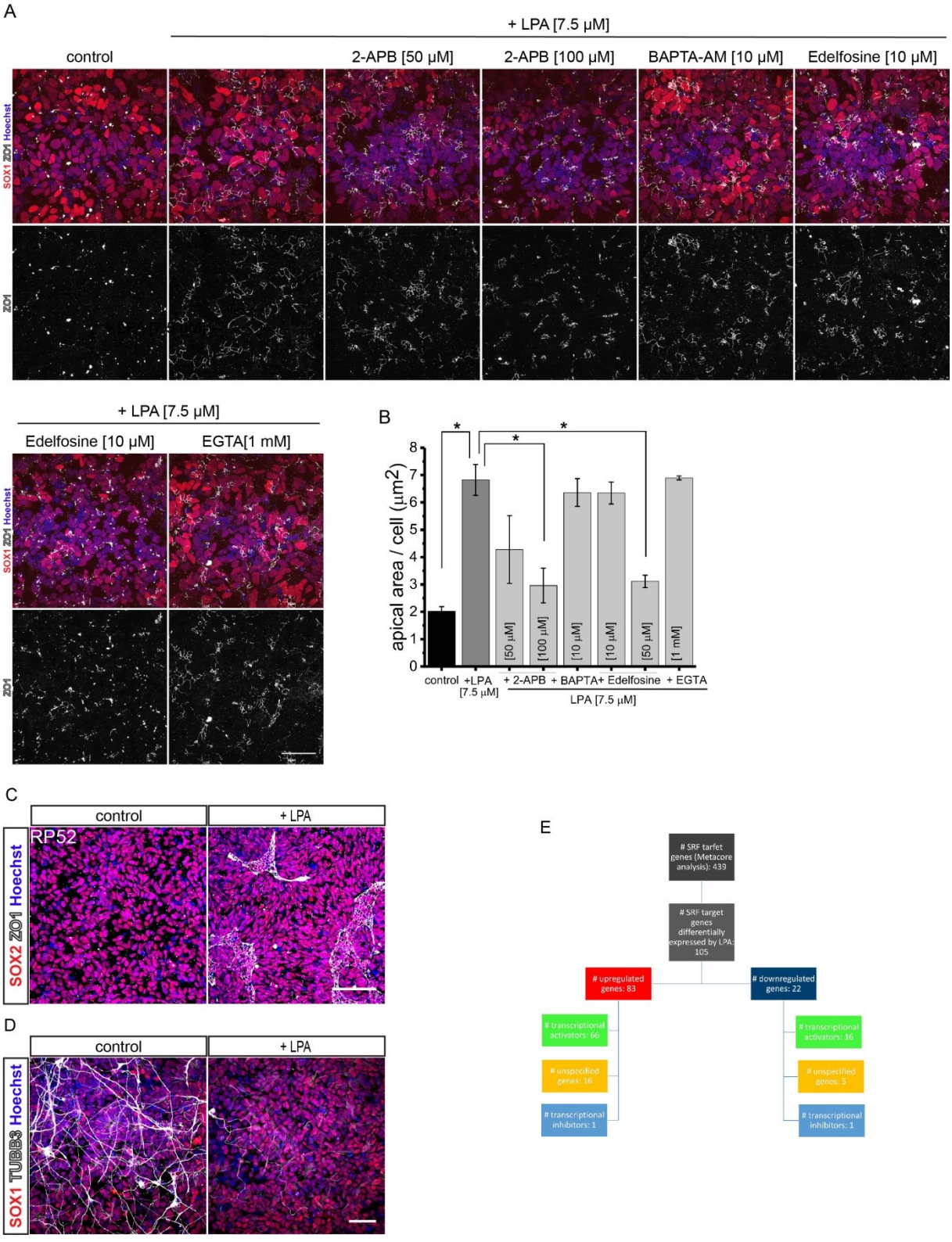

Figure S5. Characterization of the neural stem cell responses to LPA. **Related to Figure 4, Figure 5 and Discussion.** (A) Testing of a Ca^{2+} requirement for responding to LPA. Immunostaining of NPCs for SOX2 and ZO-1 that were incubated for 5 h without (control), in the presence of LPA [7.5 µM] or additionally with 2-APB (Abcam, Cat. No. 120124), BAPTA-AM (Abcam, Cat. No. 120503), Edelfosine (Tocris, Cat. No. 3022) and EGTA (VWR, Cat. No. 03779). Nuclei were stained with Hoechst 33342. Scale bar is 50 µm. (B) Quantification of the apical area per cell in μm^2. Statistical significance was analyzed using an ANOVA test followed by a Tukey a posteriori test. * $p < 0.05$, n = 3 independent experiments (C) Constant LPA exposure maintains the

large rosette morphology of HESC-derived NPCs. Immunofluorescence of NPCs that have constantly been cultured in culturing medium (control) or medium supplemented with 1 - 2 µM LPA (+ LPA) for 52 passages. NPCs were immunostained for SOX2 and ZO-1. Scale bar is 100 µm. (D) Constant LPA exposure prevents neuronal differentiation of NPCs. Immunostaining of RP1 NPCs that had been cultured in normal culturing medium or medium supplemented with LPA [0.5 µM] for SOX1, ZO-1 and TUBB3. All nuclei were stained with Hoechst 33342. Scale bar is 50 µm. (E) Metacore analysis of SRF binding targets. Experimentally known SRF target genes were retrieved from MetaCore using differentially expressed genes from the microarray analysis as input.

Supplemental Experimental Procedures

LPA assays. Related to Figure 1 – 5 and Figure S2 – S5.

To investigate the effect of LPA on HESC-derived NPCs, cells at different rosette passaging numbers were treated with different concentrations of LPA or serum. Depending on the experimental setup LPA concentrations ranging from 0.1 µM to 30 µM or 20 % FBS were added to a volume of 0.5 ml or 2 ml medium in plastic- or glass bottom 24-well plates (Corning, Greiner). The applied LPA concentration for each experiment is generally indicated in the main text, in the figure legend of the respective figure. NPCs were exposed for different time periods to LPA ranging from 2 h to 36 h. NPCs shown in Figure 1, Figure 2E, Figure 3A, Figure 5A, Figure S2, Figure S3 (middle right panel) and Figure S4 were incubated for 2 – 24 h with different LPA concentrations in a volume of 0.5 ml medium. NPCs shown in Figure 3B, 3C and Figure 4O were incubated for 10 h in the presence of LPA in 0.5 ml or 2 ml medium. Cells shown in Figure 4C and Figure S3 (upper panels) were exposed for 8 h and 12 h in 2 ml medium to 10 µM and 3 µM LPA, respectively. Cells shown in Figure S5A were incubated for 5 h with LPA in 2 ml medium. NPCs presented in Figure 4N were incubated for 10 h in 2 ml of media volume and 1µM LPA. Long-term exposure of the NPCs to LPA (Figure 2A, Figure 3E and 3F, Figures 5B, 5C and 5G, Figure S5C and S5D) was performed by incubating the cells with different LPA concentrations for several days. To achieve more stable LPA concentrations in the medium throughout the incubation time we increased the culture medium volume from 0.5 ml to 2 ml per well, thereby quadruplicating the amount of total LPA molecules per well to ameliorate the effects of LPA depletion and in addition, renewed the medium every 6 h (Figure 3E and 3F), every 12 h (Figure 2A, Figure 5C, upper and middle panels, Figure S5D) or every 24 h (Figure 5B, 5C, lower panels, 5G and Figure S5C).

Fitting the two-state model to the data of apical domain size *per* cell. Related to Figure 3.

We analyzed the apical domain size *per* cell versus LPA concentrations with a two-state model. Briefly, the model assumes that LPA concentration ([*LPA*]) drives the apical domain size from a minimal value A_{min} to a maximal value A_{max}, according to the following differential equation:

$$\frac{dA}{d[LPA]} = k(A_{max} - A) \qquad \text{(Eq. 1)}$$

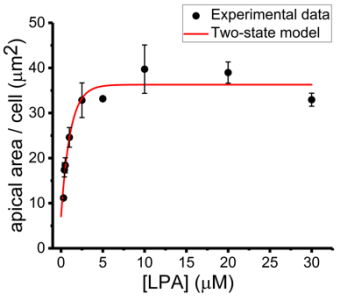

With the initial condition:

$$A([LPA] = 0) = A_{min} \qquad \text{(Eq. 2)}$$

The analytical solution is:

$$A([LPA]) = A_{max} - (A_{max} - A_{min})e^{-k[LPA]} \qquad \text{(Eq. 3)}$$

From Eq. 3 we calculated the [*LPA*] that would be necessary to achieve the 50 % of the difference between the maximal and the minimal apical domain size per cell ($[LPA]_{50}$) as follows:

$$[LPA]_{50} = \ln\left(\left(\frac{1}{2}\right)^{\frac{1}{k}}\right) \qquad \text{(Eq. 4)}$$

We fitted a two-state model to the experimental data (Figure 3G) and found that $[LPA]_{50}$ is 0.766 µM, a concentration that is in agreement with the range of physiological LPA concentrations present in serum (Yung et al., 2014).

Primary antibodies used in this study. Related to Figure 1 – 5 and Figure S1-S5.

goat anti-SOX1 (1:100, R&D Systems), goat anti-SOX2 (1:100, R&D Systems), mouse anti-SRF (1:100, Merck Millipore), rabbit anti-N-cadherin (1:100, Santa Cruz Biotechnology), rabbit anti-PKC (1:100, Santa Cruz Biotechnology), mouse anti-ZO-1 (1:150, BD Biosciences), rabbit anti ZO-1 (1:100, Thermo Fisher Scientific), rabbit anti-Vimentin (1:500, Abcam), rabbit anti-Nestin (1:500, Abcam), mouse anti-Prominin-1 (1:25, Miltenyi Biotec), mouse anti-betaIII-tubulin (TUBB3, 1:700, R&D Systems), mouse anti-GFAP (1:500, Merck Millipore), mouse anti-HuC/HuD (1:50, Thermo Fisher Scientific), rabbit anti- active Caspase 3 (1:800, Abcam), rabbit anti-phospho histone H3 (1:400, Merck Millipore), mouse-anti c-cadherin (1:20, DSHB).

Secondary antibodies used in this study. Related to Figure 1 -5 and Figure S1-S5.

Secondary antibodies used in this study were as follows: Alexa Fluor 488 donkey anti-rabbit IgG (1:200, Invitrogen), Alexa Fluor 647 donkey anti-mouse IgG (1:200, Invitrogen), Cy3- donkey anti-goat IgG (1:100, Dianova). Nuclei were stained with Hoechst 33342 (1-5 µg/ml, Sigma). F-actin staining was performed by adding Alexa Fluor 488 Phalloidin (1:200, Invitrogen). Phalloidin was added for 30 minutes to the cells and removed together with the secondary antibodies.

Microarray analysis and GO term functional annotation clustering of upregulated genes. Related to Figure 4.

RNA from three independent experiments was used to perform Agilent One-Color Microarray-Based Gene Expression Analysis (version 6.5) according to the manufacturer's instructions (Agilent Technologies). Briefly, for each sample 90 ng total RNA (derived from RP2 control small-rosette NPCs and NPCs treated with 25 µM LPA) was used to reverse transcribe double stranded cDNA and subsequently in-vitro transcribe Cy3-labeled target cRNA with the Low Input Quick Amp Labeling Kit (Agilent Technologies). The target cRNAs were hybridized to SurePrint G3 Human GE 8×60K Microarrays (AMADID 039494, Agilent Technologies). Scanned images were analysed with the Feature Extraction software 10.7.1.1 (Agilent Technologies) using default parameters (protocol: GE1_107_Sep09, grid: 039494_D_F_20120628) to obtain background-corrected signal intensities. The data were further analysed with the GeneSpring GX Software (Version 13.0, Agilent Technologies), where quantile normalization of the data and removal of unreliable signal intensities (filtering of data by expression: in three out of six experiments the signal intensity of a probe had to be above the 20th percentile to be retained in the data set) were performed. For statistical analysis a one-way ANOVA analysis with a p-value cutoff of 0.05 was performed. Gene ontology (GO) functional annotation clustering of the genes which were significantly up- or downregulated (> two-fold) in the presence of LPA was performed using DAVID software (https://david.ncifcrf.gov/, version 6.8). For functional annotation clustering the GO cellular component database (GO_CC_all) was used. Analysis classification stringency was set to medium. The microarray data shown in this paper have been uploaded to the Gene Expression Omnibus (GEO) database (https://www.ncbi.nlm.nih.gov/geo/query/acc.cgi?acc=GSE111597).

Measurement and blockage of cell proliferation. Related to Figure 2.

For measurement of the proliferative activity of the cells, NPCs were incubated for 45 min with 30 µM 5-ethynyl-2'-deoxyuridine (EdU) prior to fixation. EdU was detected by the Click-iT® Alexa Fluor 488 imaging kit (Invitrogen). The procedure was performed according to the manual´s instructions. Cell proliferation was blocked using hydroxyurea (HU) (Sigma-Aldrich). NPCs were incubated for 12 and another 18 h with 0.5 µM HU in medium or medium supplemented with LPA.